TOPICAL REVIEW • OPEN ACCESS

Integrated photonic devices in single crystal diamond

IOP Publishing J. Phys. Photonics 2 (2020) 042001 https://doi.org/10.1088/2515-7647/aba171

Journal of Physics: Photonics

Integrated photonic devices in single crystal diamond

Sichen Mi, Marcell Kiss, Teodoro Graziosi and Niels Quack

École Polytechnique Fédérale de Lausanne, 1015, Lausanne, Switzerland

E-mail: niels.quack@epfl.ch

Keywords: single crystal diamond, photonic integrated circuit, color center, quantum photonics, diamond photonics, microfabrication

OPEN ACCESS

RECEIVED
15 December 2019

REVISED
7 March 2020

ACCEPTED FOR PUBLICATION
30 June 2020

PUBLISHED
3 August 2020

Abstract

The field of diamond photonics is reviewed, with a focus on recent experimental demonstrations of photonic integrated devices in a single crystal diamond. This field leverages the outstanding material properties of diamond with the aim to establish large-scale integrated photonics for applications in sensing, information and communication technologies, and optomechanics. Accordingly, this review introduces recent progress in scalable micro- and nano-fabrication techniques for single crystal diamond photonic integrated devices, and provides quantitative comparative evaluation of the performance of the state of the art devices. The review concludes with an outlook of the potential of photonic integrated circuits in single crystal diamond.

1. Introduction

Diamond has long been recognized as an exceptional material featuring outstanding mechanical, thermal and optical properties [1]. Benefiting from this unique combination of material properties, many diamond-based applications have been demonstrated, such as spectroscopy in harsh environments[2, 3], Raman lasers from DUV to mid-IR [4–7], and beam combining amplifiers working in the kilowatts regime [8]. Beside the advantageous properties listed in table 1, an important stimulus that boosted researchers' interest in diamond photonics is the discovery of stable, room-temperature single photon emission from color centers hosted in single crystal diamond [9], as single photon sources (SPSs) are the enabling building block for a variety of quantum technologies in imaging, computing, and communication.

Color centers are point defects in solid that can absorb photons in the visible range, which in sufficient concentration give rise to colorization of diamond crystals, and are therefore termed as such. Although hundreds of different kinds of such defects have been documented for natural and synthetic diamond [10, 11], only a few have been extensively studied. Among them, the most well-known is nitrogen-vacancy (NV) center, whose structure is shown in figure 1. Understanding and harnessing their properties has given rise to numerous novel applications of diamond photonics. For example, NV centers have been used for magnetic and current sensing with nanometre spatial resolution [12, 13], for keeping quantum information at room-temperature with duration exceeding 1 second [14], and for establishing quantum entanglement between distant electron spins [15]. Following these successes, there has been an increasingly active community working on the monolithic integration of single-photon sources, low-loss waveguides, modulators and photodetectors towards the establishment of diamond integrated photonics platforms, aiming at shrinking the footprint and at the same time scaling up the system complexity. These efforts can be expected to lead to manufacturable and scalable quantum photonic circuits in diamond, in analogy to the tremendous developments that have been witnessed over the past decades for modern computing and communication infrastructures enabled by silicon photonic integrated circuits (PIC).

In this review we focus on experimentally demonstrated diamond PIC components with an operating wavelength in the range from visible to telecommunication wavelengths in the near infrared, motivated by the typical emission wavelength of color centers in the visible range, and as the interface to existing telecommunication infrastructures is paramount for wide-spread adoption of diamond photonics [23, 24]. We here focus on the review of photonic devices fabricated in single crystal diamond (SCD). Although integrated photonic devices have been demonstrated in polycrystalline diamond as well, the performance in polycrystalline diamond will be inferior to single crystal diamond devices. For example, the propagation loss will be higher for polycrystalline diamond waveguides due to scattering at grain boundaries and increased surface roughness, and the grain boundaries in poly-diamond will lead to higher background noise in single

Table 1. Material Properties of single crystal diamond and nanocrystalline diamond compared to single crystal silicon. For each value the reference is reported in the square parenthesis.

Property	Single Crystal Diamond	Nanocrystalline Diamond	Single Crystal Silicon
Young's Modulus (GPa)	1080–1155 [16]	500–1120 [17]	165 [18]
Hardness (GPa)	50–110 [16]	35 - 98 [17]	13 [19]
Density (kg m^{-3})	3520 [20]	3300–3510 [17]	2330 [20]
Thermal Conductivity ($Wm^{-1}K^{-1}$)	2200 [20]	12–1370 [17]	140 [20]
Thermal Expansion Coefficient (K^{-1})	0.8–0.9$\times$ 10^{-6} [16]		2.6$\times$ 10^{-6} [21]
Sound Velocity (m s^{-1})	18 000–19 000 [16]	15 700–17 980 [17]	8300 [20]
Raman Shift (cm^{-1})	1332 [16]		520 [22]
Bandgap (eV)	5.47 [20]		1.12 [20]
Transparency Range (μ m)	0.22 - 20 [20]		1.1 - 6.5 [20]
Refractive Index	2.4 [20]		3.5 [20]

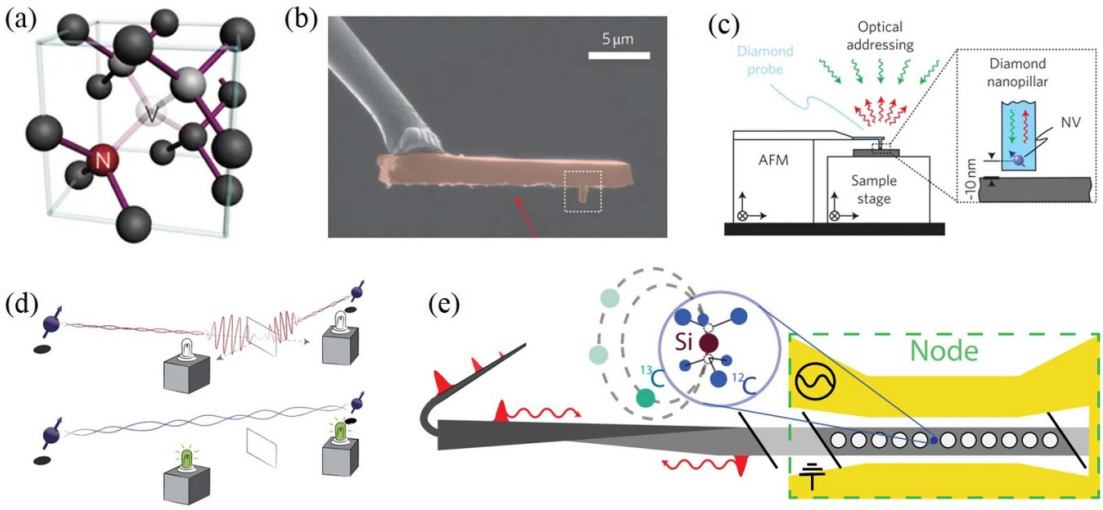

Figure 1. (a) A NV center consists of one vacancy and one substitutional nitrogen atom in diamond carbon lattice [26]; (b) scanning probe made of diamond for nanoscale magnetic sensing, where a NV center resides in the dotted-line marked tip and the false-coloured region is SCD [27]; (c) apparatus schematic for using NV center incorporated diamond probe with AFM [27]; (d) scheme for entanglement generation from distant NV centers [28]; (e) Fiber-interfaced integrated quantum register using SiV center and neighbouring ^{13}C atom [29].

photon sources. Hybrid structures such as GaP-on-diamond [25] or similar platforms, where light is not guided in diamond but in a material structured on top of a planar diamond surface, will not be covered in great detail, since this configuration will yield limited coupling of the color centers emission into cavity modes, which are an essential requirement for emission enhancement.

In section 2 we address the current status of growth and preparation methods of SCD substrates, and we summarize the micro- and nanofabrication methods for SCD-based PIC component manufacturing. Section 3 provides a gallery of recently demonstrated state-of-the-art integrated photonic devices in single crystal diamond. We provide quantitative assessment of the reported device performance and discuss challenges in section 4, with an outlook for the potential future of diamond photonic integrated circuits in section 5.

2. Diamond micro- and nano-structuring

Mechanical hardness, chemical inertness and high refractive index are among the material properties that make diamond superior to other materials. Meanwhile, precisely these properties make the micro- and nano-structuring in return highly challenging. In this section we review the technologies that have been developed for fabricating integrated diamond photonic devices, bearing the goal of application in scalable (quantum) integrated photonics. In section 2.1 and 2.1 we give a brief overview of SCD growth methods and surface preparation, as they are the starting point of large-scale PIC manufacturing, and are important for understanding restrictions or limitations in device fabrication. Next we discuss about thin membrane fabrication in section 2.3 and device structuring in section 2.4. As color centers in diamond promise a bright future for quantum technologies, we also cover a selected set of general methods in section 2.5 for engineering such defects in a controllable fashion.

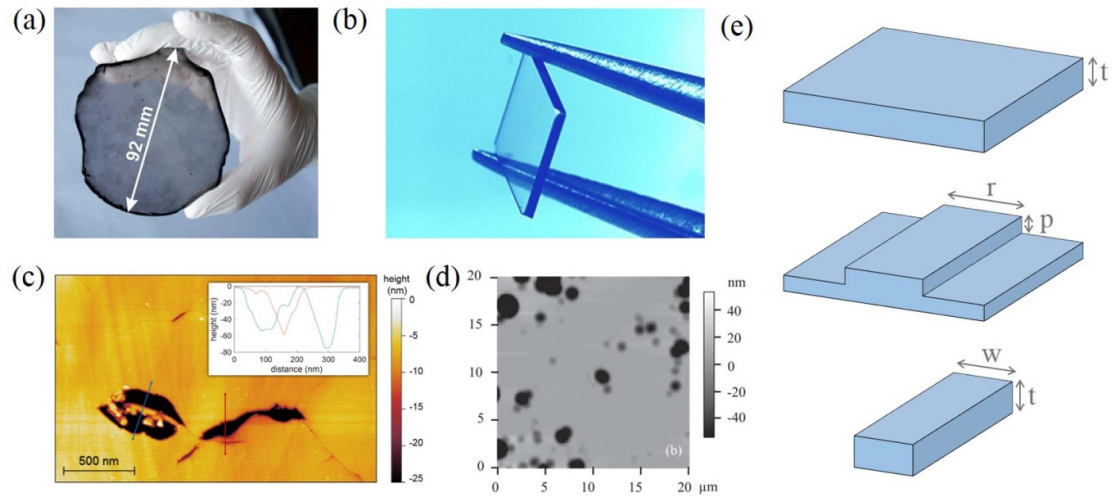

Figure 2. (a) Unpolished heteroepitaxial grown freestanding SCD wafer with 92 mm diameter. The growth was carried out on Ir/YSZ/Si(001) substrate in a 915 MHz microwave plasma CVD setup [48]. (b) Mechanically polished SCD substrate with side-length on the order of several millimeters. (c) AFM (atomic force microscopy) characterization of a commercially available SCD substrate. Mechanical polishing induced surface damage is found abundant, along with polishing lines [49] (d) After dry etching, polishing induced damages on diamond surface is exacerbated as observed by AFM [50, 51]. (e) Slab, rib and strip waveguides (from top to bottom) are the most commonly employed geometries for confining light on chip. Design dimensions for waveguides in diamond surrounded by air or silica include the total thickness t, the width of the strip w, and the partial etch depth p and width of the rib waveguide r. These are in general application dependent, and are both a function of wavelength and refractive index. As a guideline, for UV, visible and near-infrared, single- or few-mode operation will typically require t, w, p and r between 200 nm and 500 nm with excellent dimensional control at the single digit nanometer scale and surface roughness below 1 nm.

2.1. Substrate growth

Most commercial SCD substrates are grown either by high pressure high temperature (HPHT) method [30] or by homoepitaxial chemical vapor deposition (CVD) [31]. SCD grown by HPHT can achieve extremely low dislocation density [32], but it is difficult to manage impurity incorporation, and such impurities are usually distributed inhomogeneously, leading to unpredictable local variation of material properties [33]. In addition, the size of HPHT diamond is inherently limited by the growth apparatus [34, 35], therefore unsuitable for wafer production and hence large-scale integration. On the other hand, homoepitaxial CVD growth offers much better control over impurity incorporation by tuning the growth chemistry, being able to provide high quality SCD substrates suitable for diamond optoelectronic applications. 2-inch substrates can be obtained by CVD homoepitaxy on tiled arrays of seed substrates [35, 36], the resulting mosaic wafers having bonding boundaries originating from the gaps between tiles. It has been argued that such boundaries are of minor concern if they correspond to dicing lines [37] after device fabrication, while they nevertheless impose additional restrictions onto subsequent processing [35] due to, for example, compromised fracture toughness. The size limitation for CVD homoepitaxy is set by the diameter of plasma discharge, which can be extended by appropriately developed designs utilising microwave excitation of lower frequency [36, 38].

Very recently, diamond growth by heteroepitaxial CVD has also shown promising progress, with dislocation density reaching the regime of homoepitaxy SCD [39]. The dislocations can reveal etch-pits [40] during device fabrication, and even when invisible they still cause local strain and affects the optical properties of diamond such as birefringence [41, 42]. Stronger defect-related electroluminescence was also shown for p-i-n diode fabricated from heteroepitaxial grown diamond compare to that from HPHT diamond [43]. The pronounced advantage of heteroepitaxy is the potential to manufacture wafer-sized SCD substrates directly on a different material, greatly easing wafer separation and subsequent processes. A record sized 92 mm diameter SCD wafer has been demonstrated based on heteroepitaxial growth on silicon handle wafers with iridium-based buffer layers, as shown in figure 2. The suitability of such wafers for quantum sensing has been assessed recently [44].

CVD growth of diamond is also compatible with patterned or structured substrates, yielding the potential to directly grow diamond photonic micro-/nano-structures [45–47]. However such bottom-up approaches are likely to introduce impurities in an uncontrolled or unfavorable way. In the following we will thus focus on top-down approaches, while re-growth of a thin layer by CVD can in certain cases provide distinct advantages, with examples given in section 2.3.

2.2. Surface preparation

Being a high refractive index material, the dimensional requirements on diamond waveguiding structures are very stringent. In particular, the waveguiding layer has to be thin enough to guarantee single- or few-mode operation for various PIC functionalities. Tight confinement of light and sharp contrast in refractive indices impose further strict requirements on the surface quality of photonic structures. For low-loss waveguides and high-Q optical resonators in the visible and telecommunication wavelength, surface roughness below 1 nm r.m.s. is usually required [52, 53].

As-grown SCD material typically presents a rough surface, which necessitates planarization and smoothening processes prior to further processing. Crystal growth methods that realize near-perfect as-grown diamond surfaces have been investigated, yet either with low to moderate yield and limited surface area [54], or at the cost of very slow growth rates [55]. As a result, polishing of rough as-grown or laser-cut surfaces still prevails for diamond surface preparation. Usually these treatments are carried out by mechanical means, and consequently result in undesired process-induced damage to the pristine material [50, 51, 53]. For example, surface defects that typically exist in commercially available substrates are clearly seen in figure 2, and severely limit fabrication yield. Although careful fine-polishing can limit the density and magnitude of such defects [50], the extreme hardness and brittleness of SCD also make it very difficult to avoid subsurface damages [41] formed during mechanical polishing, whose presence causes detrimental effects for applications in electronics, quantum information processing and precision sensing. Unlike surface damages that can be readily identified by optical microscopy, characterizing subsurface damage typically involves more advanced characterization techniques [56]. To date, the precise extent of subsurface damage remains elusive, and is estimated from sub-micron [57] to 10 μm deep sample volumes [58]. To avoid potential device failure caused by polishing induced subsurface crystal damage, a few microns of diamond material are usually removed by plasma etching before further structuring [50, 52, 53].

Apart from causing damage, traditional mechanical polishing techniques are not suitable for large-area processing of SCD wafers due to the strong anisotropy and brittleness of diamond, especially when the wafer is thin, risking fracture. To mitigate these challenges, a variety of novel polishing techniques have been developed [41, 49, 59]. For polishing the aforementioned mosaic wafers [37], efficient processes with little-to-no mechanical load are particularly important [35, 49]. Since homoepitaxial growth remains currently the most reliable way for high quality SCD growth, we also note that fine polishing of seed diamond plates gives much improved crystalline quality of CVD growth layer [41], highlighting the importance of polishing techniques for the manufacturing of high quality single crystal diamond substrates. For a more comprehensive review on diamond polishing and surface preparation, interested readers are referred to reference [57, 60].

2.3. Membrane fabrication

Photonic integrated devices require confinement of the optical mode both in vertical as well as in lateral directions, which is achieved by providing refractive index contrast. Typical wave-guiding structures require a thin film or structured strip of material surrounded by another material of lower refractive index. Most commonly exploited waveguide geometries include slab, rib and strip waveguides. In order to achieve single- or few-mode operation for a given wavelength λ, the dimensions have the be chosen accordingly. For diamond surrounded by air or silica, the critical dimensions are typically smaller than λ, i.e. for UV, visible and near-infrared, typically between 200 nm and 500 nm with excellent dimensional control at the single digit nanometer scale. The schematics of these structures are shown in figure 2.

A suitable approach to fabricate waveguiding structures is to structure a thin film of single crystalline waveguiding material on a low refractive material. Technological developments have perfected this approach for Silicon Photonics by manufacturing specialized silicon-on-insulator (SOI) wafers using a crystalline layer transfer technique (SmartCut). A similar approach has more recently been successfully demonstrated for wafer-scale lithium-niobate-on-insulator substrates, and the suitability of this approach for diamond-on-insulator (DOI) substrates has been postulated. It is important to note, that silicon-on-diamond structures have also been studied, where diamond replaces the insulator layer, yet these do not constitute diamond-on-insulator substrates per se. DOI substrates consist of a (single crystal) diamond layer, on top of a low refractive index dielectric layer, for example silica, which is typically on top of a thick silicon handle layer. In addition to requirements on the thickness to a few hundreds of nanometers dictated by the aim for single-mode operation, the diamond layer has to be of high quality, in particular with low surface (and for structured waveguides: sidewall) roughness to minimize propagation losses.

The quest for diamond photonics relies thus heavily on the establishment of a high quality (single crystal) diamond-on-insulator technology. Yet although tremendous advances have been achieved in the past decade,

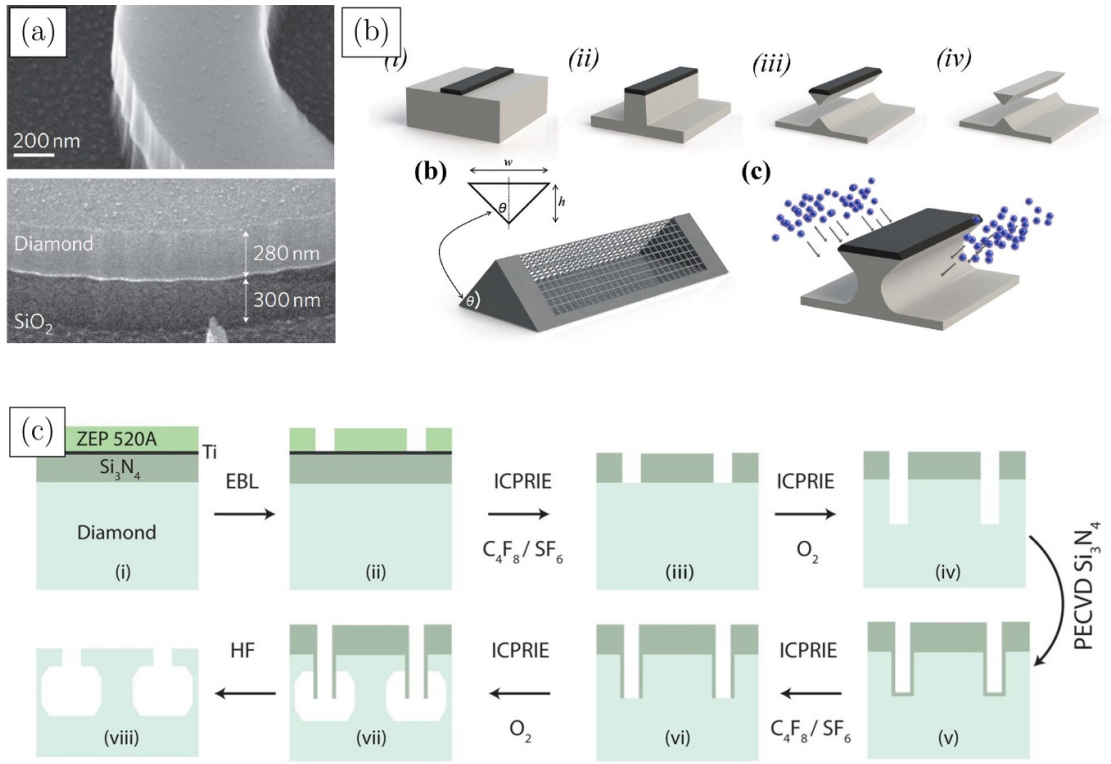

Figure 3. Typical fabrication techniques for integrated diamond photonics. (a) Typical diamond-on-insulator structures. A thin diamond membrane is formed on or attached to an insulating layer, typically SiO_2, which is then patterned into devices using lithography and dry etching [64]. (b) "Angled etching" via a Faraday cage produces undercut if combined an initial vertical etching, enabling free standing structures with a triangular cross-section [65]. (c) Quasi-isotropic etching uses an unbiased oxygen plasma for crystal plane selective etching, enabling undercuts similarly to the SCREAM process in silicon [66].

the demonstration of large-scale diamond-on-insulator substrates remains today elusive. In the following, the recent developments towards the goal of large-scale diamond-on-insulator substrates are reviewed.

Conceptually, the most straightforward method of fabricating a diamond thin film on an insulating layer is the direct growth of diamond. The challenge for this approach lies however in the production of a high quality thin film, due to the aggressive growth conditions for diamond and the difficulty of heteroepitaxy. While there has been significant success in single crystal diamond heteroepitaxy [44, 48], this approach requires a complex support stack to accommodate for lattice mismatch between the substrate and diamond, which has to date proven prohibitive for direct growth of diamond on insulator. Growth of polycrystalline diamond on insulator however has been demonstrated, yet yielding low quality thin films [61–63].

Thin diamond films can also be fabricated by thinning bulk crystals. Here, the challenge is in manipulating the thinned membrane and achieving uniformity and smoothness along the dimensions of the membrane. Recently, membranes as thin as 5μ m became available for commercial purchase [67, 68], which makes them an attractive starting point for fabrication of diamond photonic integrated devices: subsequent thinning by reactive ion etching can produce films thin enough to support single mode propagation [64, 69], which can also be combined with silicon devices via layer transfer [70].

A promising method for achieving thin diamond single crystal diamond films employs a fabrication scheme similar to the SmartCut® process for SOI wafers. Following the first report on achieving diamond membrane lift-off via implantation by Parikh *et al* [71], there have been many publications investigating ion implantation induced graphitisation and using this phenomenon to fabricate single crystal diamond membranes and membrane-based structures. The diamond substrate is implanted with high energy (hundred keV - few MeV) light ions (He^+,C^+,O^+) to produce a buried layer rich in vacancies. High temperature annealing (500 to 1100 $^\circ$C) converts the damaged layer into etchable amorphous carbon, while simultaneously recovering some of the ion damage in the top diamond layer. The top layer can also be overgrown at this stage with pristine diamond, potentially incorporating dopants. The diamond membrane can then be released by etching the amorphous carbon layer, via chemical [72] or electrochemical [73] methods. The resulting membrane can be thinned to remove the most damaged regions [74], or attached to a frame to facilitate handling [75].

2.4. Diamond photonic device structuring

The photonic devices are structured by the etching of the diamond bulk or thin-film, based on a mask realized using lithographic techniques, typically electron beam lithography.

Due to the outstanding chemical stability of diamond and the high binding energy of C-C bonds, wet etchants typically cannot supply sufficient energy to break bonds and form etch byproducts. One known method of wet etching is to utilise molten salts, like KNO_3[76] or K_{2CO3} [77] at very high temperatures ($600^{\circ}C_+$). In this case, oxygen from KNO_3 reacts with the carbon in diamond, resulting in chemical etching (with crystallographic anisotropy). However this method is highly aggressive, incompatible with most cleanroom processes and difficult to carry out in a microfabrication environment.

Metal-catalytic etching was observed for metals with high carbon solubility (e.g. Fe, Ni). When such metals are deposited onto the diamond, carbon can be dissolved into the metal, transported to the metal-air interface and desorbed as gas. This technique is exploited as a form of polishing called hot lapping. Diamond patterning via this technique was reported by Ralchenko *et al* [78]. Iron is shown as producing the highest etch rate, 8 μm min^{-1} which is significantly faster than typical plasma etches, but the etch does not produce a smooth surface. This technique can be used for nanopatterning by the use of nanoparticles [79]. In a more recent work, Nagai *et al* also report extremely high etch rate (8.7 μm min^{-1}) for Ni catalytic etching [80]. The etch demonstrated for (100) substrates is strongly anisotropic, showing selectivity over crystalline planes.

Etching of diamond structures is also possible through directional plasma etching. In this case, the etching has a physical component, which is supplied by ion bombardment and a possible chemical component, where the ion species react with carbon atoms. The research into the structuring of diamond via dry etching concentrates on different aspects: etch rate, selectivity, verticality, sidewall and etch floor smoothness.

Oxygen chemistry is very effective in removing diamond material [81] and is typically used as a high-etch rate processing step [82]. It can be effectively combined with argon for an increase in etch rate, at the expense of mask selectivity [83]. A drawback of oxygen/argon based etches is micromasking, i.e. the erosion, and subsequent redeposition of the masking material onto the etch surface, where it prevents the proceeding of the etch. To combat this effect, the chemistry can be altered to include a gas that chemically etches the masking material [84]. Due to the typical use of oxide-based mask, adding a fluorine-containing gas is an attractive option, especially since this gas is commonly available due to it is use in Si micromachining [85]. Modifying the chemistry can also be used to alter the shape of the etched features [86].

Chlorine chemistry diamond etching has been reported to improve smoothness of the surface during etching, and has been used for polishing [82, 87]. Chlorine-based chemistries also exhibit a lower selectivity against typical particle contaminants (oxides) and against photoresist, which enables proportional etching, where low selectivity is desired [88].

A unique modification of the dry etching was demonstrated by Burek *et al* where an angled Faraday cage was used to deflect the ion trajectories [65]. Ion beam milling is also possible for a purely physical etch [89], while ion beam polishing was shown by Mi et al. [49]. The drawback of ion beam patterning is the low selectivity of the process due to the small etch rate for diamond (an advantage for polishing applications however) and the resputtering of the masking material and diamond on the sidewalls (also called fencing). An interesting improvement can be the use of reactive ion beam etching with oxygen, demonstrated by Atikian et al. for the ion milling of free-standing structures [90].

Some etch methods of crystalline materials are sensitive to the crystalline face being etched and exhibit a difference in etch rate for these faces. Such methods are extensively used in machining 3D microstructures from silicon [91] and are termed "crystallographic", to distinguish from directional anisotropy arising from ion bombardment typically encountered in dry etching. Crystallographic plasma etching was reported that was selective for dislocations [92, 93], yet the analogue of the Si crystallographic etching was first reported by Khanaliloo et al. [66]. The crystallographic etching is carried out in a standard deep reactive (ICP) ion etcher. The process is performed at high ICP powers and zero platen/bias power. This results in an almost thermal plasma (due to the missing ion acceleration) that is very dense (due to the high ICP power). In this sense, the etching performed is almost completely chemical in nature, thereby showing selectivity over the crystal orientation of the etched material. Several reports also exploit an elevated temperature to increase the etch rate [66, 94]. Process pressure is also higher than typical dry etches for the same reason (15 m Torr to 22 m Torr), however etch rates remain typically limited (< 10 mm min^{-1}) and are non-linear for undercuts [66]. Further characterisation of this etch method was carried out by Xie et al. [95].

Focused ion beam (FIB) microfabrication is an attractive alternative to plasma etching for forming 3D structures, owing to the high degree of freedom it offers [96, 97]. The samples are mounted on a multi-axis stage, allowing machining at different angles, the ion beam can be precisely focused, allowing for high resolution. The sample can be imaged by the focused ion beam, but typical FIB systems include a scanning electron microscope column as well, which allows for even higher resolution and more convenient imaging.

Bulk properties can also be changed locally to create refractive index contrast. A promising technique is femtosecond laser bulk modification of diamond, which can be used to write waveguiding structures into bulk diamond [98]. Waveguides can also be formed by implantation induced refractive index change [99].

2.5. Color center engineering

For integrated diamond photonic device fabrication, formation of color centers in SCD with quantitative and positional control is of great importance. Depending on the electronic structures of different color centers, additional specific treatments might be required to further improve their properties. In this section we briefly address commonly explored approaches for engineering of color centers in diamond, with a focus on applicable methods for integrated diamond photonics. Dedicated review articles have further previously been published on NV centers [100, 101] and group-IV centers [102].

2.5.1. Ion implantation

Ion implantation is a widely used technique for introducing foreign atoms into host materials [103]. For available ion sources, either broad-beam or focused ions can be accelerated towards the diamond substrate, and depending on the kinetic energy, the accelerated ions gradually slow down and stop in the diamond at a depth range that can be estimated by Monte Carlo simulation [104]. Interaction between ions and target material can distort the pristine sp^3 carbon crystal lattice structure, creating vacancies and carbon self-interstitials. When stopped, the ions either replace native carbon in the lattice (substitutional impurities), or reside in interstitial position. At this stage the crystalline structure can be heavily damaged, and GR1 signal can be generally observed, indicating the creation of vacancies. Post-implantation annealing [105] at high temperature restores (to a certain extent) the lattice structure and mobilizes vacancies, which can then be trapped by impurities, forming impurity-vacancy complexes, such as NV centers. For practical applications, nevertheless, formation of certain defects may not be sufficient; properties such as long coherence time and small spectral diffusion are often important. This additional requirements make ion implantation less suitable for certain applications. For example, a recent study [106] implanting ^{15}N into diamond with native nitrogen incorporation demonstrated that implantation-introduced nitrogen atoms tend to form NV^- centers with drastically compromised optical coherence compared to their native counterpart, possibly owing to local damage caused by implantation. HPHT annealing has been shown to narrow the emission linewidth of NV^- ensembles [107] fabricated by implantation, but further study is required to better understand the underlying mechanisms. SiV^- centers on the other hand, show decent optical coherence when fabricated by implantation and post-annealing, in both bulk and nanostructured diamond [108, 109]. In the absence of post-annealing, creation of NV^- centers has been observed after swift heavy ion implantation [110]. Electronic excitations and thermal spikes were suggested to be possible mechanisms for color center formation, yet further investigations are required to understand this process.

The prominent advantage of implantation for color center fabrication is the positional control. The incident position of ions can be confined to nanometer precision by using focused ion beam [111], masks with nano-holes [112], or pierced AFM tips [113]. The depth distribution of the stopped ions is determined by their initial kinetic energy: increased implantation energies result thus in less accurate positioning. The lateral straggling follows the same trend. For example, nitrogen implantation with 2.5 keV acceleration can reach 10 nm accuracy, while for 10 keV it is about 30 nm [114]. Consequently, precise positioning the color center deep into the substrate is not possible with direct ion implantation. This can be nevertheless be circumvented by shallow implantation followed by overgrowth [114–116]. Another approach for three-dimensional positioning is laser writing which will be addressed in section 2.5.3. Combining delta-doping and electron irradiation can also be used to realize 3D positioning, and will be discussed in 2.5.4. A caveat regarding ion implantation in single crystal materials are ion channelling effects, which can occur upon implantation at specific angles with respect to the crystal orientation, and has been shown to result in greatly extended ion implantation depths compared to Monte Carlo simulations [117]. Therefore, best practices for ion implantation is to avoid implantation at certain angles, depending on the crystalline plane orientation.

Quantitative control of defect density can also be achieved by adequately increasing or decreasing the implantation dose, however, typically careful calibration is required to precisely control the resulting defect density, as the conversion yield varies with experimental conditions [111, 118]. Electron and laser irradiation have further been demonstrated effective for improving the conversion yield, as will be discussed in the next sections.

2.5.2. Electron irradiation

As ion implantation causes severe lattice damage, which may degrade the performance of color centers, electron irradiation has been employed as an alternative to create vacancies [51, 119]. The threshold for

accelerated electrons displacing carbon atom in the lattice is about 150–170 keV [111, 120]. Formation of impurity-involved defects in this way relies on pre-existing foreign elements. This method for example has been used to increase the yield of SiV^- [111] and NV^- [119] formation after ion implantation, indicating that the conversion yield from implanted impurity to impurity-vacancy complex is limited by the availability of vacancies. As for ion implantation, lateral positioning can also be achieved with electron irradiation [121]. Meanwhile, MeV electrons can travel through mm-thick diamond and are therefore suitable for modifying the properties of bulk diamond. It is interesting to note that electron irradiation with energy below the threshold for vacancy creation [120] has been shown to also promote the formation of NV^- centers in a nitrogen-implanted sample, possibly due to electronic excitation.

2.5.3. Laser irradiation

Direct lasing writing for fabricating color centers has been intensively studied in recent years, and the fast progress has shown great promise in terms of flexibility, quality and conversion yield [122–126].

In 2013, Liu *et al* [123] demonstrated that femtosecond laser pulses can be used to ionize molecules in air, with the resulting electrons accelerated by subsequent pulses towards the diamond surface, creating vacancies. Following annealing, photoluminescence from NV^- centers can be observed. The starting material was type Ib diamond with abundant nitrogen impurities, and it is not clear if there were nitrogen ions accelerated and implanted into the diamond. In 2019, the same group reported formation of SiV^- centers using a similar method [122], but with silicon nanoballs coated on high-purity diamond surface. The results unambiguously shows that Si ions were accelerated by the laser pulse and implanted into diamond.

Another approach is to focus a laser pulse directly into bulk diamond with native impurities. Photoluminescence from GR1 centers confirmed photo-generated vacancies. Following annealing, NV^- centers with good optical coherence were observed [124]. The same group later also found out that thermal annealing can be replaced by laser irradiation itself [125]. A first pulse was applied to generate vacancies in the crystal, which was followed by a pulse train with lower energy, to locally anneal diamond at the focus spot. In this way one can observe photoluminescence signal from the same spot in real time, and stop the laser annealing with the onset of NV^- formation. This method provides excellent control of the NV^- formation process, and the authors report an impressive yield of 96% for creating single NV^- centers. In addition, it has also been demonstrated that this method is well suited to fabricate 3D arrays of color centers [126], showing much greater flexibility over ion implantation.

2.5.4. CVD growth

Color centers can be incorporated directly into diamond during CVD growth. For example with the presence of nickle in the CVD chamber, NE8 center can be observed in as-grown diamond [127, 128], while ion implantation so far has been demonstrated unsuccessful for its creation [129, 130]. Furthermore, CVD growth is of particular interest for the preferential orientation of color centers [131], which is important for various applications such as metrology [132]. Very recently, record-long inhomogeneous spin-dephasing time ($T_2^* \approx 1.5$ ms) and Hahn-echo spin-coherence time ($T_2 \approx 2.4$ ms) were found for NV^- center in a phosphorus-doped CVD diamond [133], leading to better sensitivity for magnetic sensing. Isotopic engineering of CVD diamond by tuning growth condition can also improve the coherence properties of color centers [134].

In general, the impurities incorporated during CVD growth present relatively inhomogeneous distribution. However, in the particular approach of "delta doping" foreign atoms can be introduced into the diamond at a specified depth [135], even with perfect alignment [131]. In combination with electron irradiation, positional control in 3D has also been demonstrated [121].

2.5.5. HPHT growth

Similar to CVD doping, impurities can also be incorporated into diamond during HPHT growth. They usually originate from the environment (e.g. nitrogen) or the solvent-catalyst (e.g. nickle) used to dissolve carbon, and it is not trivial to make this process under precisely controlled conditions. Like CVD growth, preferentially aligned NV centers have been observed in HPHT grown diamond [136]. Since HPHT growth is more difficult to control than CVD, quantitative engineering of color centers using this method seems unlikely at this moment.

2.5.6. Charge state control

The control of the charge state is of importance for several applications. For example, NV centers exhibit ODMR only when negatively charged [137] therefore NV^- centers have been extensively studied for magnetic sensing, and the spin coherence time of neutrally charged SiV centers largely exceeds the one of

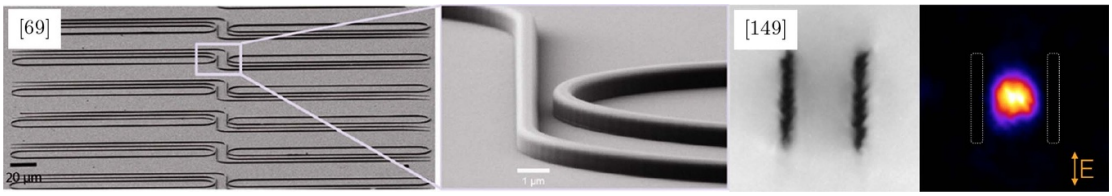

Figure 4. Waveguides in single crystal diamond fabricated via membrane thinning [69] or direct laser writing [149].

negatively charged ones [138] since total spin of 1/2 makes SiV^- prone to phonon-mediated, dynamic Jahn-Teller–like orbital relaxation [139].

The charge state of color centers can be passively engineered by doping, which modifies the Fermi level of diamond, leading to preference in forming a certain charge state. In 2016, Doi *et al* showed that CVD-grown diamond, n-doped with phosphorus, has steady state population of NV^- above 99% under 593 nm illumination, leading to enhanced luminescence and magnetic sensing [140]. Implantation of Si ions into boron-doped CVD diamond showed > 80% conversion yield to SiV^0 as the Fermi level was pinned to make neutral charge state have the lowest formation energy [138]. Doping by implantation of phosphorous and boron followed by high temperature annealing has also been demonstrated effective to change the charge state of NV centers [141]. Apart from doping, annealing in dark has been reported to convert SiV from neutral to negative state [142]. HPHT annealing at 8 GPa and 2000 degrees increases the NV^-/NV^0 ratio by a factor of 5, but this is accompanied by an overall decrease in the NV count [107]. Better understanding of this process requires more knowledge on the interplay between color centers and donors/acceptors during annealing. For near-surface color centers, the chemical termination of diamond surface also plays a role in determining the charge state [141, 143, 144]. Active control of the charge state has been demonstrated by optical [145] or electrical means [146]. Approaches to achieve charge state control at device-level are discussed in section 3.7.

3. Review of diamond photonic integrated devices

In this section we review integrated photonic devices that have been fabricated in diamond.

3.1. Waveguiding Devices

Guiding light between photonic devices in a well controlled manner with limited losses requires the fabrication of waveguiding structures. In this section, diamond waveguide approaches are shown, along with other passive optical structures, such as splitters and couplers. Although theoretical investigations of such high-index contrast structures in diamond have been performed (e.g. [147, 148]), only fabricated devices will be discussed.

Angled etching is a versatile technique capable of creating very high-quality waveguides with a triangular cross-section [52], with an estimated propagation loss of 1.5 dB cm−1. With the use of a broad ion beam to instead of a Faraday-cage, difficulties arising from misalignment of the sample with respect to the Faraday cage can be mitigated, while keeping the advantageous properties [90, 150].

A promising method for fabricating waveguiding structures is ultrafast pulsed laser-based structuring. Here the most common structure is referred to as Type II structure comprising two parallel written lines providing confinement to the optical mode. Such waveguides were initially high loss with 7.9 dB cm−1 [149] and 16 dB cm−1 [151], but significant improvements have been demonstrated 4.2 dB cm−1 [152]. Other passive optical structures, such as Y-splitters (-7 dB) and bends (3 dB bend loss for radius of 25 mm) have been demonstrated [149]. These techniques are also applicable for MIR applications [153], with propagation losses of 6 dB cm−1 at 2.4 μ m and 8.6 μm. The confinement can also be achieved by ion implantation induced refractive index change [99], however the losses are high 22 dB cm−1 due to absorption.

Membrane thinning and subsequent patterning lends well to the fabrication of waveguides. Such diamond-on-insulator waveguides have been demonstrated with very high quality by multiple groups [69, 154, 155]. Excellent propagation losses are reported (1.7 dB cm−1 [69], 0.34 dB cm−1 [155]). The resulting waveguides can be overgrown [156, 157], with propagation losses of 16.5 dB cm−1, improved in the subsequent publication to 12.3 dB cm−1, by compensating for the membrane wedge and smoother e-beam patterning. Another possibility is the transfer of the membrane onto a SOI substrate via drop-casting, resulting in hybrid diamond—Si or diamond—HSQ – Si waveguides [70], with excellent reported propagation losses of 0.34 dB cm−1.

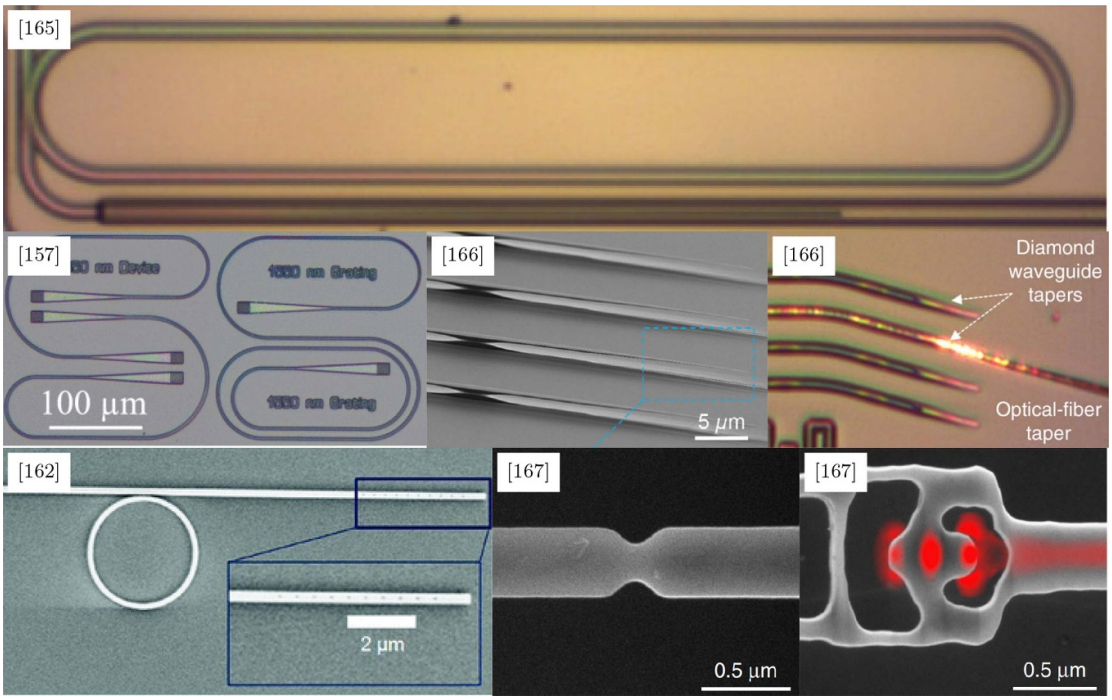

Figure 5. Racetrack cavity fabricated on a diamond-on-insulator (DOI) substrate, coupled to a waveguide which is extended by SU-8 resist to the edge of carrier substrate [164]. Grating couplers on DOI substrate operating at a central wavelength of 1550 nm [156]. SEM and optical images of suspended diamond waveguide taper fabricated with angled-etching method [165]. Second-order grating coupler on DOI waveguide [161]. Notch and inversely designed vertical coupler for quasi-isotropic etch platform [166].

Ion implantation induced graphitisation and release coupled with dry etching can be used to define free-standing [158] or membrane-based [159] waveguides. In the latter case a propagation loss of 7.2 dB cm−1 was reported. The authors comment on the possibility of the fabrication of fully etched structures on the platform by either using anchor structures or the augmentation of the membrane structure with a low refractive index material on the bottom side, such as PECVD SiO_2.

3.2. Coupling devices

Interfacing light between photonic waveguides and optical fibers (or free-space) has been demonstrated for diamond-on-insulator based devices by either butt coupling or using grating couplers. In the former case, an adiabatically tapered diamond waveguide is extended, as shown in figure 5, by SU-8 resist or spin-on glass to the edge of the sample, and both free-space [5] and lensed fiber coupling [69, 155, 160] have been demonstrated. Example grating couplers for visible [161, 162] and telecommunication [157, 163] wavelengths are also presented in figure 5.

The simplest option for coupling light to and from devices fabricated by the angled-etch method may be a notch in the waveguide, however, only very low efficiency around 1% [53] have been achieved. On the other hand, efficient (> 90%) interfacing was reported at visible and telecommunication wavelengths by adiabatic mode transfer from a diamond waveguide taper to an optical fiber taper [165]. Free-space coupling of femtosecond laser pulses to a diamond waveguide taper was also carried out in a demonstration of supercontinuum generation [167], however, the tapered section was damaged at high pump power.

Owing to a strong correlation between the initial etch depth and undercut thin-film area for quasi-isotropically etched devices, fabrication of couplers requires more design optimization. Dory *et al* [166] reported recently on the inverse design method for fabricating devices based on this fabrication approach, and the resulted vertical couplers (figure 5) showed efficiency > 24 times of that of a waveguide notch.

3.3. Optical resonators

Starting from a bulk diamond plate, direct milling with focused ion beam (FIB) is an attractive method to create 3D structures and several demonstrations of photonic structures realized with FIB milling have been reported. Bayn *et al* fabricated triangular nanobeam photonic crystal cavities by milling the bulk diamond substrates from two directions [168]. Optical characterisation reveals a *Q* factor of 221 at visible wavelengths. Similar investigation into FIB milled nanobeams are carried out by Babinec *et al* [169]. Instead of achieving a triangular cross section, a rectangular photonic crystal beam was fabricated by using milling directions

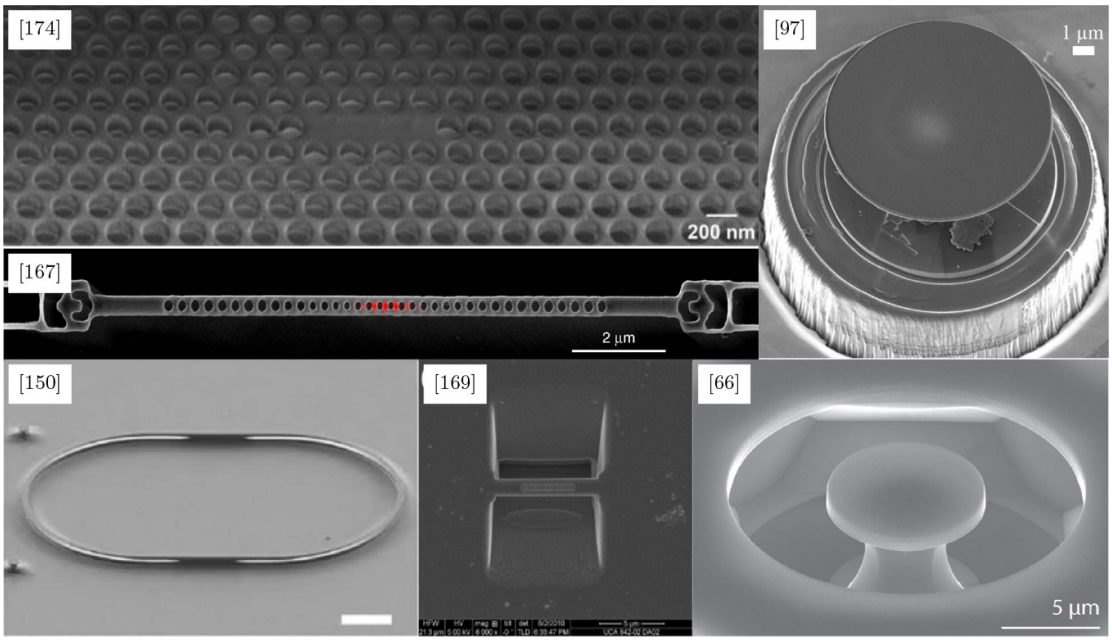

Figure 6. Microresonators fabricated in bulk single crystal diamond. Photonic crystal beam [168] and microdisk resonators [97] structured by focused ion beam milling. Racetrack resonator by angled etch [52]. Microdisk [66], 2D photonic crystal [173], and 1D photonic crystal beam fabricated by quasi-isotropic etching [166].

orthogonal to the diamond plate. An alternative fabrication scheme is also proposed, where diamond lamellas are fabricated into diamond slabs, based on the commonly used transmission electron microscope lift-off technique [170]. The authors report no Q factor measurements. FIB milling can be used in combination with reactive ion etching (RIE). One of the two techniques presented by Li *et al* [171], involves the structuring of a photonic crystal beam starting from a rectangular cuboid, patterned with the photonic crystal, which is suspended from the substrate with FIB milling. No optical Q is reported. Microdisk resonators were fabricated by Graziosi *et al* using a combination of RIE and FIB milling [97]. A pillar is defined by an initial directional oxygen reactive ion etch step, which is subsequently undercut using FIB milling from two directions. The authors report an optical Q of 5700 at telecommunication wavelengths, the highest reported quality factor by FIB machining.

In a different approach utilising directional milling (angled-etching), several photonic structures have been demonstrated, including suspended 1D photonic crystal cavities, microdisks, and suspended waveguides, operating at telecommunication and visible wavelengths [52]. Racetrack resonators feature loaded Q-factors of $Q_{TE} \sim 151\,000$ and $Q_{TM} \sim 113\,000$ at 1550 nm wavelength. Further evolution of this technique employed etching by a broad ion beam and rotation of the tilted sample to achieve similar undercutting [90]. The method, termed reactive ion beam angled etching, uses an oxygen ion beam to mill the surface. Atikian *et al* demonstrate racetrack resonators in polycrystalline diamond ($Q \sim 30\,000$) and single crystal diamond ($Q \sim 286\,000$). Uniformity is demonstrated by fabricating two racetrack resonators separated by 19 mm, with comparable quality factors and transmission spectra.

Crystallographic etching, also referred as quasi-isotropic etching has successfully been employed to fabricate microdisks and photonic crystal beams and membranes. Khanaliloo *et al* presented single crystal diamond microdisks of $\sim 1\mu$ m thickness and $\sim 7\mu$ m diameter, with a faceted supporting pillar of $\sim 4.6\mu$ m. Optical characterisation reveals a loaded Q of $\sim 1.091\,0^5$ [66]. After extensive process optimisation, Q was improved even further by a factor ~ 4 [172]. The authors investigated optimising the hard mask etching step, the anisotropic vertical diamond etch step, surface treatment and cleaning and the modification of the pedestal shape via an additional masking layer. Mouradian *et al* applied the crystallographic etching to fabricate nanobeam cavities in single crystal diamond [94]. Optical measurements reveal an optical Q factor above 14 700 at visible wavelength. Dory *et al* [166] have demonstrated nanobeam photonic crystal cavities using similar techniques, achieving Q factors of 4000 at NV center wavelengths. The fabrication process for nanobeam cavities was subsequently extended to fabricate 2-dimensional photonic crystals by Wan *et al* [173]. With a practically equivalent process flow, $\sim 4\mu$ m-wide, ~ 200 nm-thick planar slabs are fabricated, with optical cavities formed by designed defects in photonic crystal. The measured Q factor is from 2670 to 6080 at 637 nm.

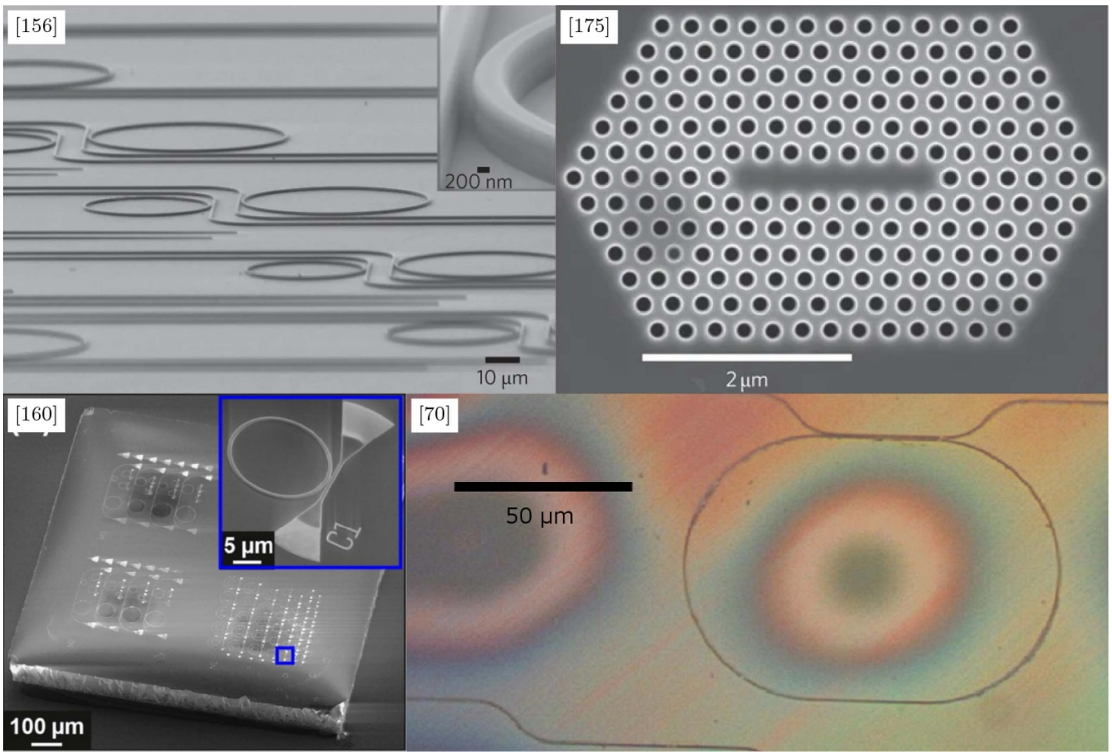

Figure 7. Single crystal diamond resonators fabricated in thin film diamond. Microrings coupled to waveguides [155]. 2D photonic crystal cavity in a heteroepitaxially grown single crystal diamond thin film [174]. Photonic circuits, including microring resonators [159]. Single crystal diamond thin film on top of silicon waveguides and microring resonators (adapted from [70]).

The examples listed above are demonstration of optical cavities in bulk diamond substrates. To achieve the vertical confinement, undercut is necessary to create a low index region below the resonators. Substantial development has been reported for the fabrication of thin diamond membranes and of photonic devices on diamond thin films. Improvements are demonstrated in growing the diamond layer by utilising an iridium buffer layer for growth by Riedrich-Möller *et al* [174]. By engineering the lattice mismatch of the growth substrate (Ir/YSZ/Si(001)), the grown ~ 12μ m thick layer is single crystal diamond, even if rich in dislocations. To fabricate free standing membranes, the backside silicon layer is etched in windows using deep reactive ion etching. The buffer layers are removed via ion beam etching, and the diamond film is thinned, removing the lowest quality nucleation layers. Subsequently, FIB milling is carried out to pattern the layer into nanobeams and photonic crystal cavities. A final annealing at 1000 $^{\circ}$C is carried out for 2 h in vacuum, followed by an acid treatment (H_2SO_4:H_2O_2, 1:1) and oxidation (420 $^{\circ}$C, 2 h), to remove FIB damage. *Q* factors of 700 and 450 at visible wavelength are reported for the 1D and 2D photonic crystals, respectively.

Faraon *et al* demonstrated a fabrication of a single crystal diamond-on-insulator type structure by thinning a 5 μ m membrane [64]. The fabricated microring resonators have a *Q* factor of 5000, limited by sidewall roughness. A similar process flow was carried out by Hausmann *et al* [69]. Large diameter ring resonators and racetrack resonators have been fabricated, with a measured *Q* of ~ 250 000. This fabrication process was adapted for suspended structures later by the same group [175], with a Si substrate. Cavity modes are measured for the released nanobeams with *Q* factors up to ~ 6000. Two dimensional photonic crystal cavities are fabricated based on a similar process flow by Jung *et al* attaching a thin single crystal diamond membrane onto a Si substrate [176] and using focused ion beam milling to create the holes for a photonic crystal structure. The authors report a *Q* factor of 870 at 637 nm. Similarly thinned membranes are used by Li *et al* as well [177]. Photonic crystal cavities were fabricated and characterized, yielding *Q* values of 4700 at 632.3 nm. This fabrication method was later used by Schröder *et al* to fabricate 2D photonic crystals [111] with embedded Si vacancies, by local implantation via Si focused ion beam. Hill *et al* demonstrated the integration of a thin diamond membrane with a Si photonic integrated circuit [70]. Hybrid Si—diamond and Si—HSQ – diamond waveguides and resonators were fabricated via this method. The authors report ~ 30 800 for structures with and ~ 10 800 without HSQ.

Single crystal membranes fabricated by ion implantation and sacrifical layer etching (diamond Smart Cut, see section 2.3), have served as substrates for fabrication of photonic devices [159]. Rib-type photonic structures were characterised optically and a (loaded) *Q*-factor of 66 000 was reported for disk resonators.

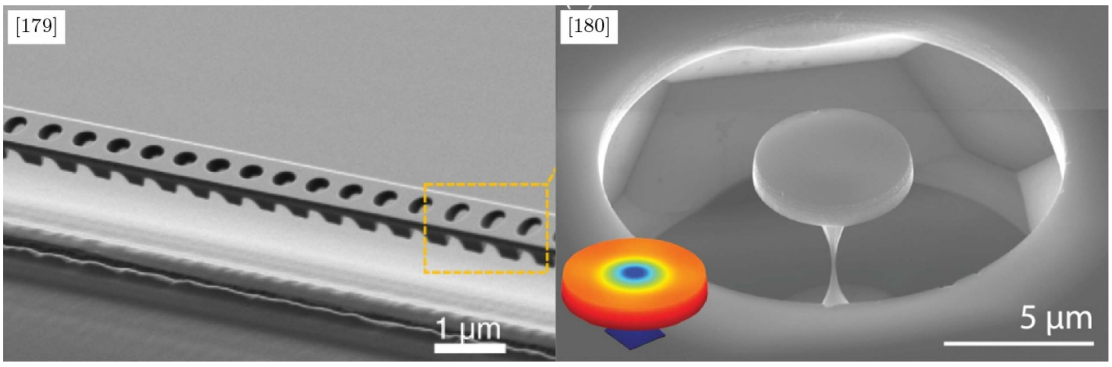

Figure 8. Optomechanical resonators in single crystal diamond. Photonic crystal beam fabricated with the angled etching technique [178]. Single crystal microdisk fabricated in a bulk substrate using a quasi-isotropic undercut. [179].

3.4. Optomechanical Devices

The ability to suspend diamond optical cavities paves the way for diamond cavity optomechanics. Including a appropriately designed optomechanical crystal in an angled-etched diamond cantilever, Burek *et al* [178] demonstrated phonon lasing and Optomechanically Induced Transparency (OMIT). The devices present high optical quality factors Q_o ($1.7^{*}10^5$ and $2.7\ 10^5$) and high $\Omega/2\pi$ (5.5 GHz and 9.5 GHz), making the optomechanical cavity operate in the resolved sideband regime. Measured mechanical quality factors (at ambient conditions) are of the order of ~ 5000. Mechanical quality factors (Q_m) of diamond resonators tend to increase at lower temperatures [180], and follow-up work [181] has verified this reduced dissipation for diamond optomechanical crystals, recording an increase of 30× at 5 K, measuring Q_m up to 238 000. In combination with the high high oscillating frequency, the devices exhibit Qf-products in the order of 10^{15} Hz at 5 K (10^{13} Hz at 300 K).

The group of Paul E. Barclay at the University of Calgary presented several cavity optomechanics experiments using SCD microdisks. The fabrication strategy is based on a quasi isotropic etch [179], here yielding microdisks supported by an hourglass shaped pedestal with octagonal cross section. Self-oscillation amplification was demonstrated in SCD microdisks with sufficiently thin pedestal diameters. Mechanical resonances corresponding to the fundamental radial breathing mode are reported with $\Omega/2\pi \sim$ 2 GHz and $Q_m \sim$ 9000 (at room temperature and pressure), yielding an Qf-product of 1.910^{13} Hz. The pedestal geometry appears to be of particular importance for the RBM dissipation, and only the thinnest pedestals (~ 100 nm) present small mechanical dissipation. The microdisks show high optomechanical cooperativity $C = Ng_0^2/\kappa\Gamma \sim eq2.7$ under ambient conditions. Further work by the authors investigated fabrication strategies to improve the sidewall surface roughness, improving the optical quality factor to ~ 300 000, as well a way of reducing the mechanical dissipation by engineering the pedestal shape [172, 182]. With the engineered pedestal, demonstration of optomechanical cooling and OMIT was possible [182]. Excellent OMIT performance was reported even with $Q_o \sim 10^5$. OMIT can be further exploited using a second control laser signal to achieve all optical switching [183], optical control of pulse time storage storage[184], and optomechanically mediated wavelength conversion [185, 186].

3.5. Sources

The wide bandgap allows SCD to be used for fabricating light-emitting diodes (LED) with 5.27 eV emission due to exciton recombination [187]. Its associated transparency also permits Raman lasing operating in the DUV range [4]. However here we will only discuss diamond-based light sources in the visible-to-telecommunication range, as diamond PIC component for UV light has not been demonstrated, partially due to the fact that the high refractive index of diamond implies small feature sizes and low tolerance on fabrication errors [162, 188].

3.5.1. Single photon sources

Many color centers in diamond have been verified as single photon emitters [191]. However, due to their interaction with local field, inhomogeneous distribution of transition frequency usually exists among multiple color centers of the same kind, severely limiting the indistinguishability between photons emitted from different color centers. Even for the same color center, under illumination, the local field can undergo fluctuations and the transition frequency can be unstable. NV^- and SiV^- centers for example, are sensitive to electric fields and strain fields respectively, and local variations of such fields due to impurities and processing inevitably impedes the scalability of color center based technologies for QIP. Figure 9 provides an illustrative

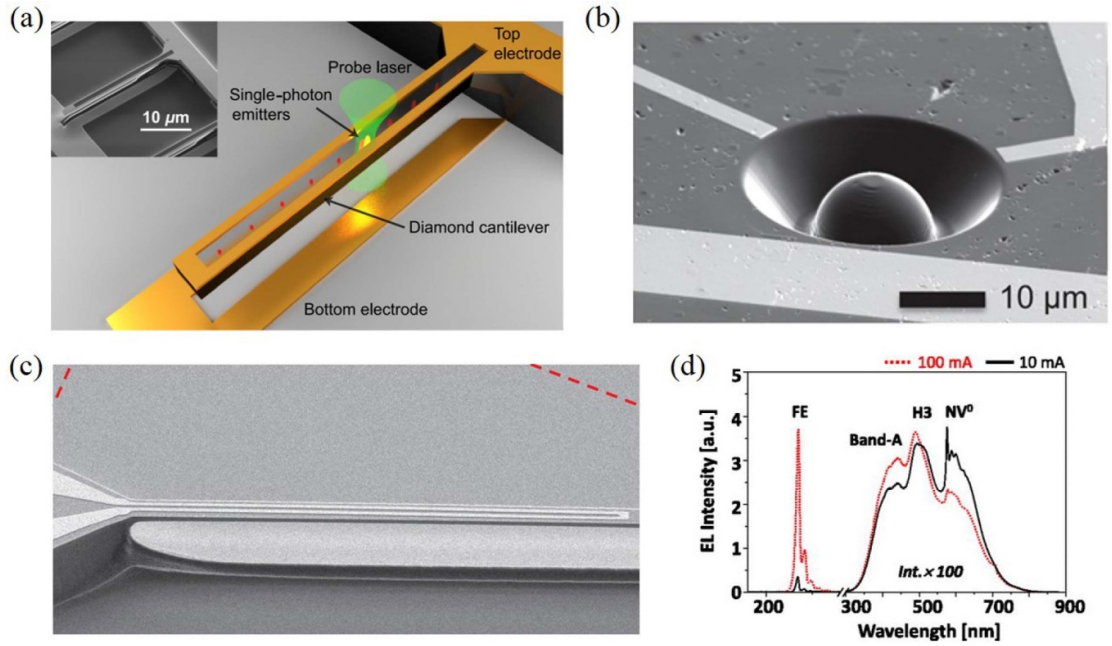

Figure 9. (a) Spectral tuning of GeV centers enabled by strain engineering [189]; (b) Electrical tuning of NV center by Stark effect [28]; (c) SNSPD integrated on SCD waveguide; (d) Emission spectra from diamond LED with dislocation defects, H3 centers and NV^0 centers, covering whole visible range [190].

summary of demonstrated devices that are able to tune the local field and spectrally align the optical transition among different color centers. Two-photon quantum interference from separate NV^- centers was reported with the help of Stark tuning [192], and with further feedback control this technique can be used to stabilize the Zero Phonon Line (ZPL) frequency of NV^- for several minutes [193]. On the other hand, SiV^- centers can be spectrally aligned and stabilized via strain engineering [194, 195], with a ZPL tuning range about 5 times the associated inhomogenous distribution in nanostructured diamond. Spin coherence time of SiV^- was also reported to be improved in this way [196]. Since group-IV color centers share a similar electronic structure [102], it is not surprising that strain tuning is also effective to align GeV centers [189].

In order to prepare quantum entanglement [15] and to generate flying qubit efficiently, high counting rate is of great practical importance [197], and the limiting factors are multifold. Fast decay time and high quantum efficiency are preferred for single photon emission, but in bulk diamond they are largely determined by the electronic structure and local environment of color centers. An effective solution is to leverage the Purcell effect, where color centers are placed in photonic nanocavities with high Q/V ratio. On photonic devices obtained by the angled-etching method, Zhang *et al* [198] demonstrated a 10-fold lifetime reduction and 42-fold emission enhancement with Purcell factor >26 when the resonance frequency of nanobeam cavity is tuned to the optical transition of SiV centers. In SCD membranes, the modification of quantum efficiency has been reported for SiV centers coupled to 2D photonic crystal cavities [199]. On diamond-on-insulator devices, observation of the Purcell effect was reported for ring resonators incorporating NV^- centers [200]. The small branching ratio into the ZPL can also be mitigated in this way, with an estimated increase from 0.03 to 0.25 [201] for a moderate cavity Q factor.

An important step towards scaling diamond quantum technology is to couple single photons directly into well-defined spatiotemporal modes. The trade-off between cavity enhancement and coupling efficiency has been discussed in [202] to maximize single photon counting coupled to guided spatial modes. Burek *et al* have demonstrated record-high coherent single photon counting rate (38 kHz) in diamond by placing SiV center in a nanobeam cavity directly coupled to a waveguide, which is further interfaced with an optical fiber [166].

As with a planar diamond-air interface a large fraction of single photon emission is reflected back into the diamond and can not reach the detectors, modification of emission pattern has also been proven an efficient way for improving count rate. A variety of structures have been demonstrated, such as parabolic reflectors [203], bullseye gratings [204], and nanowires [205]. It is also possible to integrate a diamond membrane into a miniaturized Fabry-Pérot cavity [206] to realize Purcell enhancement. Nevertheless these approaches appear not to be compatible with diamond PIC integration and are thus not within the scope of this review.

Aforementioned SPSs are all driven by optical pumping, which has to be filtered out for practical use to avoid false signals and detector saturation. Up to now the only electrically driven single photon source was demonstrated with NV^0 center in p-i-n diodes [207, 208]. Although SiV^- centers are known to emit single photons, and their electroluminescence has been observed [209, 210], an electrically driven SiV^- single photon source remains yet to be demonstrated.

3.5.2. Light emitting diodes

LEDs made from SCD have been reported at different operation wavelengths, from DUV due to exciton recombination [187], to visible and near-IR due to various defects. Electroluminescence due to dislocation (A-band) [190, 211, 212], Ni-related centers [211], H3 [190, 211], NV^0 [190, 207, 208, 211], SiV^- [209, 210], and Xe-related [213] centers has been observed. In nitrogen-rich diamond, it is common that multiple kinds of color centers and a high degree of dislocations can be found simultaneously. LEDs made from such diamonds can emit light covering the whole visible range, as shown in figure 9. No sign of electroluminescence from NV^- or SiV^0 has been observed. The p-type diamond is usually realized by boron doping, and n-type by lithium [211, 213] or phosphorus [208] doping. Both CVD doping and ion implantation have been shown successful for fabricating LEDs. So far there has been no report on LED that is directly coupled to a SCD waveguide. The experimental demonstration of such a device will be an important contribution for on-chip light source integration.

3.5.3. Supercontinuum

Supercontinuum generation (SCG) has enabled numerous applications from molecular sensing to precision metrology. Very recently the group of Loncar at Harvard has demonstrated the first SCG in diamond waveguides obtained by the angled etch method, with an output spectrum spanning from 670 nm–920 nm [167]. The group-velocity dispersion can be engineered by changing the etching angle, and thanks to the wide transparency of diamond, SGC in the UV range should be possible. However the attempt to extend SCG into UV range has hitherto not proven successful due to laser pulse induced damage on the coupling interface.

3.5.4. Raman laser

Due to the wide transparency window and large Raman gain of diamond, Raman lasers in SCD from DUV to mid-infrared have been demonstrated with a bulk cavity [4, 7] or with a monolithic coating of diamond [6]. The first on-chip Raman laser in diamond was fabricated on a DOI device [164] with a tunable range of 100 nm around 2 μm and with output power >250 μW. Later another integrated Raman laser based on the same fabrication approach with an output around 875 nm and 1.2 mW maximum power was also demonstrated by the same group [5].

3.5.5. Color center laser

The first reported color center laser in SCD dates back to 1985 when Rand and DeShazer demonstrated lasing with H3 centers as gain medium using natural diamond [214, 215]. Later Nakashima and Yazu reported H3 laser in synthetic type-Ib diamond where boron doping was carried out to increase the density of H3 centers [216]. A few more H3 lasers were documented in reference [217, 218] including a continuous-wave laser with output around 540 nm and tunable bandwidth (3 dB) about 40 nm. However all of these experiments employed bulky optics. Since then no successful color center lasing was reported [219, 220], and although of high interest for integrated diamond photonics, the demonstration of on-chip integrated color center lasing in single crystal diamond remains elusive.

3.6. Detectors

The wide band-gap of diamond renders it an excellent candidate for detecting UV light, and offers several orders of discrimination between deep UV and visible light [221]. This advantage allows recent developments for example in solar-blind imaging [222] and optical communication [223] using diamond-based UV detectors. On the other hand, since the intrinsic absorption [224] for visible-IR photons by high quality SCD is negligible, defects have to be present for all-diamond photodetecting devices [225]. Although possible in principle, the photodetection sensitivity for this wavelength range is generally quite low, mostly with A/W (Ampere/Watt) responsivity below 1×10^{-5} [226]. An exceptionally high responsivity of 1×10^{-2} A/W for for green light was reported [227] yet no clear explanation for the high responsivity was provided. Improved performance for visible-IR photon detection is demonstrated by defect passivation [228], or by stacking NiO [229] or metal layers [226] on diamond. It is however still insufficient for quantum information applications where single photon detection is essential.

Superconducting nanowire single photon detectors (SNSPDs) fabricated directly atop diamond waveguides have been shown promising for fully integrated diamond photonics, where high sensitivity to

single photons and small footprint are realized simultaneously [230–233]. To this end, a superconducting film is deposited on diamond, and subsequently structured into different geometries. Figure 9 shows an example device, where a niobium titanium nitride nanowire lies directly on a suspended diamond waveguide. Guided photons evanescently couple to the nanowire, and are absorbed along propogation. Below critical temperature, the absorption of a single photon by the nanowire could induce a superconductivity breakdown, which can be registered by electrical signals due to voltage drop. So far waveguide-integrated SNSPD in SCD was only reported by Atikian *et al* [230] on devices fabricated by angled-etching, but the characterization was carried out by illuminating the nanowires from above, rather than by coupling single photons into the waveguide. The detailed fabrication process was not revealed either. Meanwhile, SNSPDs have also been demonstrated on poly-crystal DOI platform [231–233]. Since the fabrication and characterization methods can be readily ported to single-crystal DOI substrates, their performance will be addressed in section 4.6.

3.7. Other devices

Modulators are essential components towards fully functional PICs. However they have not been demonstrated in SCD. Rath *et al* [234] reported an electro-optomechanical phase shifter fabricated in polycrystalline diamond, the fabrication process of which is compatible with SCD thin films as well. The phase change of the guided optical signal was not reported though.

The native integration of color centers in diamond can further lead to devices that are beyond the conventional concept of integrated photonics. For example, devices for actively controlling the charge state of color centers have been demonstrated. Deterministic initialization of single NV center to neutrally charged state has been reported in a p-i-n diode [146], and the state can remain stable for more than 0.45 seconds (limited by measurement equipment). Without bias, NV^0s eventually return to NV^-s spontaneously [190]. In contrast, a n-i-n diamond junction was demonstrated to increase NV^- population to 80% [235]. Similarly, bias-modulated population of SiV^- was also reported in a p-i-n diode [210]. Apart from LEDs, electroluminescence of NV^0 centers has also been demonstrated with buried graphitic electrodes [236]. Noticeably, with applied bias below a certain threshold, the photoluminescence signal of NV^- increases with voltage at the expense of NV^0 population, while above threshold the conversion is reversed.

Further examples of devices regarding spin-state manipulation and readout include among others magnetic sensors by photocurrent detection of magnetic resonance (PDMR) [237–239] or acoustic and strain control of electron spins [240–243]. Theses devices deal with additional degrees of freedom other than photons and make diamond a promising material as the interface between flying qubits and solid-state quantum memories.

4. Discussion

In this section we provide a quantitative comparison of the state-of-the-art devices fabricated by different methods and discuss about future challenges.

4.1. Waveguiding devices

Efficient integrated optical systems require low-loss waveguides to transport light between devices. The operating wavelength is an obvious factor in quantifying the quality of the realized waveguiding devices, as scattering losses are related to both the wavelength and the scattering imperfections. Typically, lower propagation loss is thus observed with an increase in wavelength [244]. Another important factor is the geometry of the waveguides: low-loss waveguides are typically designed with a rib cross-section, which increases mode confinement to lessen the effect of sidewall scattering and increase compactness of the structures [245].

Of the surveyed techniques for waveguide fabrication, the most suited methods for this type of device are the diamond-on-insulator and direct writing approaches. While bulk structure methods can produce very high quality features, the limited flexibility in patterning imposes additional constraints on the achievable geometry. Long and flexible waveguides can be realized by angled etched technique, with supports underneath, which manifest small scattering loss (10^{-3} dB per support) [165], but power splitter has not been demonstrated. On the other hand, Y-splitter designs have been conceived with 95 % efficiency for quasi-isotropic etch platform [166], but long waveguide was not seen in the literature.

Diamond-on-insulator fabrication techniques follow the well established silicon photonics fabrication techniques in silicon-on-insulator substrates. As seen with silicon, rib waveguides can offer superior performance [246] compared to strip waveguides, if the additional lithography and etch step is feasible. Fabrication based on the ion cut method [159] is also a competitive option, with improvements in substrate quality via overgrowth or thinning [74].

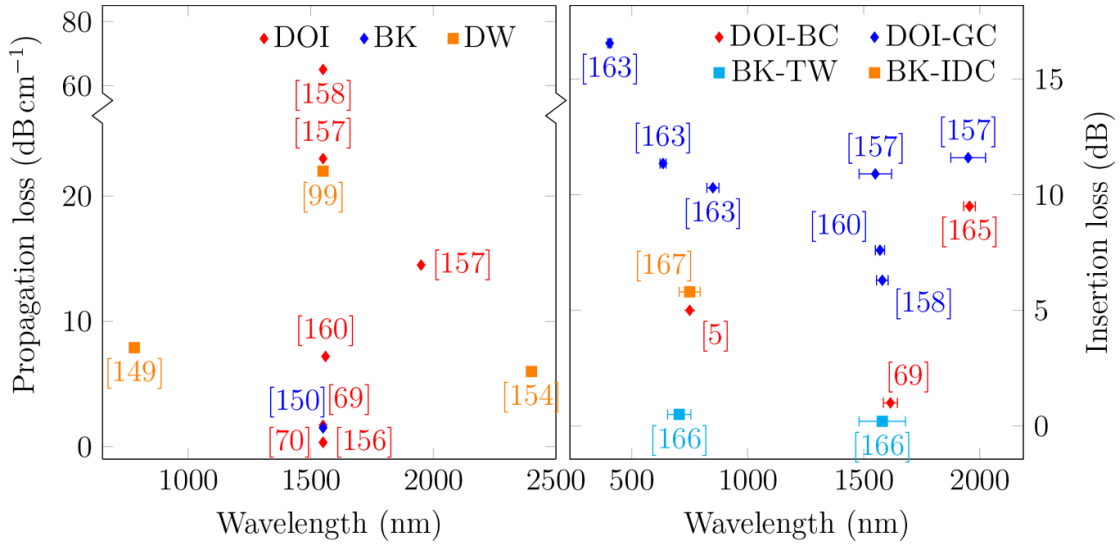

Figure 10. Left: SCD waveguides characterized by propagation loss and wavelength. Right: coupling devices characterized by insertion loss, bandwidth and wavelength. Bandwidth is not always reported specifically, and where applicable, has been extracted from reported transmission spectra. In reference [5] no data is available therefore no horizontal bar is presented here. DOI: diamond-on-insulator. BK: bulk. DW: direct writing. TW: tapered waveguide. IDC: inversely designed coupler. BC: butt-coupling. GC: grating coupler.

Direct writing offers great flexibility in fabrication, at the expense of writing time. Performance has been greatly improved in recently publications, with values rivalling DOI results [152], with other passive devices, such as bends and Y-splitters demonstrated [149], showing the viability of such devices. At the time of this review, ion implantation-based waveguides remain prohibitively lossy [99] due to absorption.

4.2. Coupling devices

Efficient coupling of light from/to photonic circuits is indispensable for developing on-chip components and eventually realizing diamond photonics based quantum networks. Depending on the target application, wavelength, bandwidth, efficiency and power-handling capacity are important aspects to consider.

As shown in figure 10, coupling components in SCD have been demonstrated for a wavelength range from 400 *nm* to 2 μm. Among them, the most efficient interface was reported by Burek *et al* [165] where a free-standing tapered diamond waveguide is interfaced to a fiber taper, and with careful design the efficiency can be made larger than 96% (91%) for telecommunication (near-IR) wavelengths. Upon coupling a free-space pulsed laser into a diamond waveguide using this interface [167], damage at the tapered region was observed at high power, highlighting the importance of further optimization for applications in this regime. Another drawback of the suspended taper interface is its fragility during fabrication [165], but further development in the processing should mitigate this challenge.

As for devices fabricated by quasi-isotropic etching, additional fabrication/design challenges arise due to the strong correlation between the undercut area of free-standing structures and the initial etch-depth. This can be partially overcome by a recently developed inverse design method where fabrication constraints are taken into consideration for design optimization [166]. With this method, the insertion loss of the fiber-to-chip coupling interface amounted to 6.8 dB for polarization-maintaining fibers and to 5.8 dB for multimode fibers.

For butt-coupling to devices fabricated in diamond-on-insulator, the insertion loss between a lensed fiber and the diamond photonic chip can be made as low as 1 dB/facet [69]. Due to limited size of the diamond thin film, the diamond waveguide was extended by spin-on glass or SU-8 resist to the edge of carrier wafer. This step also facilitated polishing of the waveguide end facet which reduces coupling loss and helps to maintain polarization. This scheme has also been used for free-space coupling of a high power laser to the circuits for on-chip Raman lasing [5]. Grating couplers operational down to 405 *nm* was demonstrated by Gao *et al* [162], and the best lowest insertion loss at telecommuniation wavelength was reported at 6.3 dB with a fully-etched strip waveguide profile [157]. Employing a partially etched rib waveguide design may help increase the performance, as has been shown for poly-DOI devices [61].

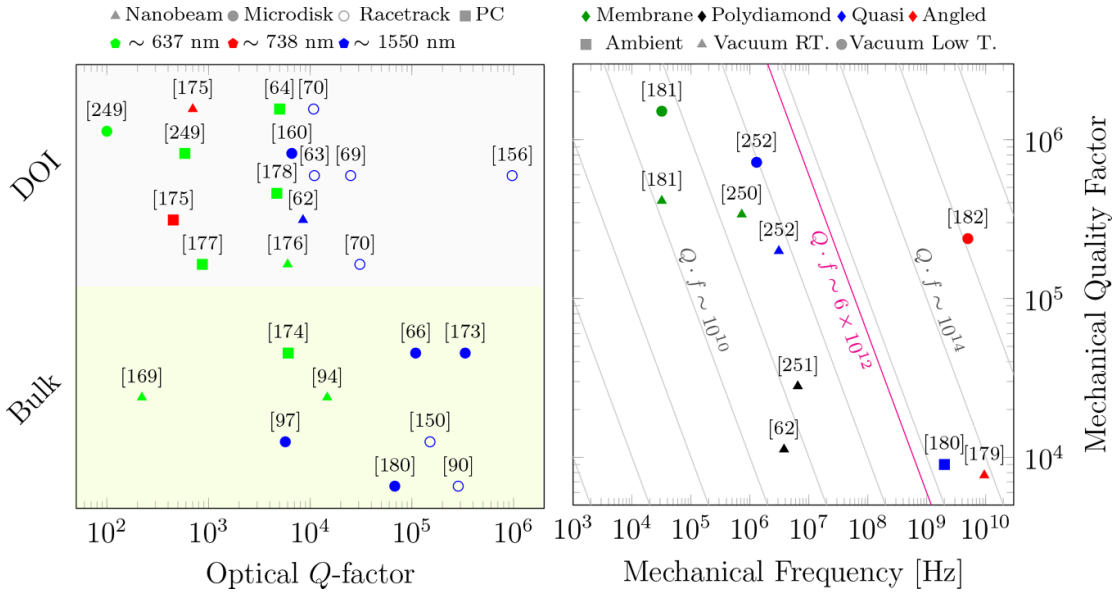

Figure 11. Left: Reported Q-factors of diamond optical resonators grouped by fabrication technique. The shape of the marker indicates resonator type, while the colour indicates the wavelength of operation. When multiple values were reported, the highest value was chosen. DOI ~ diamond-on-insulator, PC ~ photonic crystal. Right: Qf-product plot of diamond optomechanical resonators. The colors indicate the fabrication method used (Quasi ~ quasi-isotropic etch, Angled ~ angled etch), while the shape represents the characterization conditions. The reported values of devices fabricated starting from thin membranes (green) are relative to mechanical oscillators (cantilevers), and no optical cavity is present. The light grey lines indicated constant Qf values for every order of magnitude, while the magenta line shows the Qf-product corresponding to room temperature k_BT value ($\sim 6 \times 10^{12}$).

4.3. Optical resonators

The quality of optical resonators can be compared by their finesse or optical quality factor, as for most application these quantities are strongly correlated to the device performance. Figure 11 provides a quantitative comparison of the devices presented previously. Bulk diamond micromachining has been used to demonstrate the highest optical quality resonators so far, using novel 3D machining techniques [65, 66], along with flexible, but less high quality serial focused beam techniques, such as FIB [97]. The quasi-isotropic etching and the angled-etching techniques can reliably produce cavities with quality factors well in excess of 10^5, but there are limitations on the possible geometries that can be fabricated. The former is limited by the crystal orientation and relative etch rates of the diamond crystal planes. The resonator design has to take this into account. A drawback of the angled-etch method using the conical cage is the focusing of the ions during the etch process - while this makes the undercut possible due to introducing an angle to the ions, it also makes the resulting etch dependent on the positioning of the cage. Device uniformity and was improved by etching diamond with reactive ion beam angled etching [90], removing the requirement of the Faraday cage. FIB milling can affect the quality of the resonators especially due to implantation and crystal damage induced by the ion beam. Several techniques, including plasma etching, thermal annealing, or acid cleaning, were developed to alleviate or eliminate these problems. The technique cannot be easily scaled, however, and while complex structures are possible, alignment of different milling directions can induce steps or defects in the optical resonators.

Bulk diamond micromachining techniques share a limitation in the possibility of integration. Integration with metallization or other layers is challenging, since the optical confinement arises from the waveguiding structures being etched out of the substrate, rendering subsequent process steps such as lithography, etching or depositions highly challenging. However, the crystallographic etch process is commonly accessible in cleanrooms, requiring no specialized tools. Diamond-on-insulator type substrates benefit from a close analogue of their SOI counterpart, which is well studied and potentially adaptable to diamond. As demonstrated for Si, the integration of components (waveguides, resonators, couplers, conductors) is an achievable tasks. Three general categories were shown for fabricating the diamond thin film part of the DOI structure.

Direct growth of diamond on the insulator is the most straightforward method, but the grown layer will be polycrystalline in nature, which limits the achievable optical quality. While impressive results have been obtained in PCD [62], ultimately the material will limit performance. Membrane thinning can be a feasible alternative to growth, with several demonstrations of DOI structures. However, the thinning of the

membrane is a significant challenge and the resulting membranes can display significant inhomogeneity [70, 177], limiting scalability and potentially hindering further processing. While it is possible to thin a membrane from a plate, most demonstrations use few-10 μm thick membranes for starting the fabrication. These substrates are expensive and difficult to handle and ship, due to their fragility. The thickness variation can also be significant due to the elastic deformation during polishing [70]. Diamond Smart-Cut, or implantation-based lift-out is a technique studied in detail for two decades now, but has been hindered by the ion damage the substrate sustains during implantation. However, optical resonators have been demonstrated [159], along with multiple mechanical resonators, which confirm that there has been significant progress towards eliminating this ion damage. The demonstration of electronics based on this method is another vote of confidence [247]. Although this method requires access to implantation facilities, the implantation and lift-off can be parallelized and constitutes therefore an inherently scalable method, which provides excellent promise for industrial scale exploitation of diamond-on-insulator substrates.

4.4. Optomechanical devices

Figure 11 shows the Qf-product of the examples of the diamond mechanical and optomechanical oscillators presented previously. Diamond resonators can offer high mechanical quality factors, well exceeding 100 000, and appropriate geometries that yield high oscillation frequencies allow for high Qf above the 6×10^{-12} Hz threshold for room temperature operation. The high Qf values indicate that diamond mechanical and optomechanical resonators are an excellent platform to realize an optomechanical frequency references. Among the different techniques presented in this review, the angled-etching and the quasi-isotropic undercut are the fabrication strategies that have hitherto offered the highest Qf values and have shown to be better suited to realize a mechanical or optomechanical resonator to date. Both have different strengths and drawbacks, however the latter can be more flexible with regards to resonator geometries that can be realized, since cantilevers [248], 1D [166] and 2D [173] photonic crystal structures have been demonstrated. The angled etching is capable of structuring whispering gallery mode resonators, but may lack the ability to well isolate the mechanical oscillation from the substrates in the case of wide structures such as microdisks. Although no optomechanical cavity has been demonstrated to date, the creation of a thin diamond layer with implantation is also a valid approach, provided that the amorphous layer is appropriately removed to prevent mechanical losses. This can be achieved with extensive annealing [249] or by etching the layer after bonding to a scaffold [74] or to a sacrificial layer.

Extensive work has been performed to integrate color centers into mechanical and optomechanical oscillators. Given the atomic nature of the color centers, they act as a localized sensors, therefore are well suited to investigate particular phenomena[250]. Ovartchaiyapong *et al* [240], for example, proposed to use NV centers to analyze clamping losses in mechanical resonators to develop low dissipation designs. Color centers integrated in a mechanical resonators can have similar interactions as the optical and mechanical field in an optomechanical resonator, allowing for cooling and amplification of the mechanical motion [251]. As for the optomechanical system, a cooperativity and a coupling strength can be defined, which benefit from low mechanical damping and small size [243]. High cooperativity spin-mechanical systems are a fundamental building blocks of quantum networks. The mechanical field can be used both to manipulate [196, 252] and to propagate the quantum information encoded in the color center [253]. The benefit of using a mechanical oscillation compared to a magnetic field is that the former can be easily confined and guided by realizing nanostructured devices. Furthermore, optomechanical systems can be used to drive the mechanical oscillation at the characteristic GHz frequencies, and can be more efficient than other actuation schemes.

Other demonstrations of optomechanical interaction in diamond structures were reported by the group of Wolfram H. P. Pernice using a polycrystalline diamond film [62, 254]. Although mechanical, thermal and optical properties are inferior to SCD, PCD offers the great advantage of deposition on different substrates and the ability to process it with conventional microfabrication techniques, since most demonstrations of optomechanical systems, similar to other materials, which are dominantly based on thin films over a sacrificial substrate.

4.5. Sources

As discussed in section 3.5, to scale up color center based quantum technologies, devices that can spectrally align and stabilize their transitions are indispensable. The performance of these sources are summarized in table 2. We also include the Raman scattering scheme which is enabled by an external tunable laser, instead of on-chip integration of controlling components.

Although proof-of-principle demonstrations have been carried out, several challenges still remain. For SiV^- and GeV^- centers the reported devices rely on electrodes fabricated directly on top of the waveguide. For concept validations, this constitutes a suitable strategy, but if this structure is to be scaled up, long wirings could be a major source of single photons being absorbed and scattered. Strain engineering of color

Table 2. Single photon sources with the potential of individual spectral tuning. Strain field and electrical field control were demonstrated with integrated devices. Raman scheme was carried out with external laser.

Tuning Mechanism	Color Center	Ref	Tuning Range	Count Rate	Linewidth	$g^{(2)}(0)$	Temperature
Raman scattering	SiV	[165]	10 GHz	38 kHz	$\ll$ 1 GHz†	0.21	5 K
		[53]	10 GHz	15 kHz	<30 MHz†	0.16	4 K
Strain field	SiV	[195]	80 GHz		300 MHz	0.13	4 K
	GeV	[189]	144 GHz		1 GHz	0.05	50 K
Electrical field	NV	[192]	>3 GHz	2.7 kHz	<500 MHz		9 K
		[255]	> 10 GHz				20 K
		[256]	> 5 GHz		85 MHz		8 K

Note: † For the Raman scheme, the linewidth of single photons is ultimately limited by the coherence time of the spin-orbit ground states instead of the excited state lifetime of SiV^- centers [53, 139, 165].

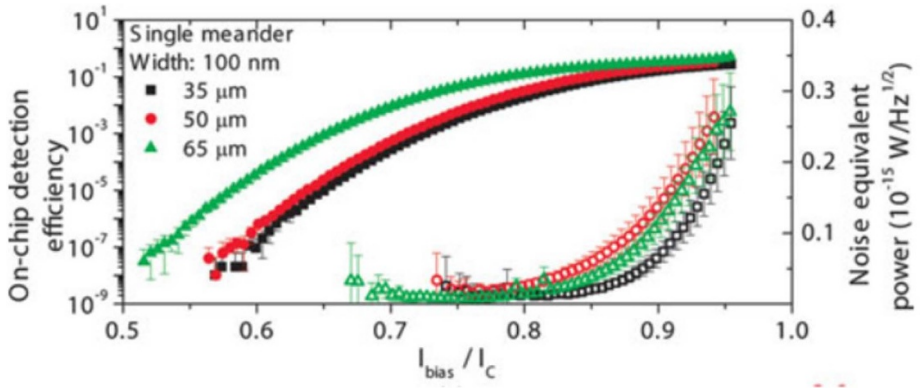

Figure 12. Typical performance of SNSPD on diamond [232]. OCDE increase with nanowire length and operating current. NEP reaches minimum in the mid-biasing region.

centers has not been demonstrated for DOI based devices, but since the supporting layer can be selectively etched away [234], this design should be readily portable. Another possible approch for strain engineering is to use a piezoelectric material for the insulator layer, such as aluminum nitride (AlN) [241]. In order to exploit Purcell enhancement, the emitter transition must be spectrally aligned to the cavity resonance, which has been achieved by gentle etching [199], atomic layer deposition [257], or gas condensation [53]. These methods however do not apply to individual cavities, and cannot be used to compensate the resonance offset due to fabrication non-uniformity. If optically pumped single photon sources are to be used for integrated quantum photonics circuits, it is also important to filter out the pump light, which can potentially be achieved by very high-Q cavities. Background fluorescence on the other hand have to be reduced by high quality growth.

On-chip integrated tunable Raman lasers were demonstrated with DOI racetrack cavities, with both pump and Stokes frequencies resonant to cavity modes [5, 164]. The lasing threshold is greatly reduced in this configuration, but the output wavelength and tunability are restricted by cavity design and by available pump laser. It will be of high interest to push the working wavelength into the visible range, for the pumping and controlling of various color centers.

With bulk optics, a tunable H3 laser was documented in reference [217], and it will be a significant contribution for diamond PIC if this can be integrated on-chip, since the emission of H3 centers in green is of interest for optical pumping of many other color centers. On the other hand, lasing of NV center has also attracted increasing attention [219, 258, 259] partially due to its potential application in magnetometry [260]. However no report on successful on-chip color centers laser in diamond has been reported in literature to date. In the case of NV center lasers, it has been suggested that photo-ionization and excited state absorption are the main challenges to overcome [219].

4.6. Photodetectors

SNSPDs that are directly integrated with diamond waveguides have only been characterized on poly-DOI devices. Nevertheless the performance of such devices, if ported to SCD, is expected to exhibit similar, if not improved, performance due to improved material and surface quality [50, 231]. Kahl *et al* [232] reported an absorption coefficient of 0.15 dB/μ m for SNSPDs, which dominates over the propogation loss of poly-DOI waveguides being 4.79 dB mm^{-1}, therefore the difference in propogation loss between waveguides made in

SCD and in polycrystalline diamond can be safely neglected in this context. Below critical temperature and critical current, SNSPDs have a typical performance as reported in figure 12. With increasing lengths of the nanowires, higher absorption and thus higher OCDE (on-chip detection efficiency) can be observed. This improvement however is at the cost of slower operation frequency, due to signal decay proportional to nanowire length. While monotonic growth of OCDE is accompanied with increased bias current, the NEP (noise equivalent power) has a global minimum in the mid-biasing region. Highest reported OCDE is 73% for 765 nm [233], and 66% for telecommunication wavelengths [231]. Surface roughness of diamond is believed to lead to constrictions [261] in the nanowires, and consequently limits critical current and therefore the detector efficiency [231]. It has also been reported that very low time jitter (down to 23 ps for telecommunication wavelengths) can be observed for devices with high critical current [233]. For future investigations it will be of high interest to further examine design optimization [262] and opportunities to exploit external fields [263, 264] to improve device performance.

5. Conclusions

Successful demonstrations of integrated Single Photon Sources (SPS), phase shifters, power splitters and Superconducting Nanowire Single Photon Detectors (SNSPD) on diamond have already provided all essential components for on-chip diamond quantum information processing via boson sampling [265, 266] and measurement-based linear optical quantum computing [267, 268]. However, hitherto, their combined integration into a single crystal diamond phtonic integrated platform remains elusive. For the angled-etch approach, the fabrication method limits the device geometry, making power splitter and phase shifter difficult to design. On the other hand, no individually tunable SPS has been demonstrated in diamond-on-insulator, which nevertheless is expected to be achievable in the short term, as discussed in section 4.5. Angled-etch and DOI platforms do not rely on crystallographic etching, and thus provide design freedom over the quasi-isotropic etch approach. For the latter case, even designing flexible routing waveguides can be difficult. Furthermore,in contrast to quasi-isotropic etching, the fabrication processes for angled-etch and DOI platforms can be readily used for SCD with different crystal-plane orientation.

The experimental demonstration of electrically driven single photon sources is a significant achievement towards fully on-chip quantum photonics circuits, yet it remains challenging to realize coherent photon emission with low background noise. In addition, if achieved, electrically driven SPS based on SiV^- centers, will be of great interest due to their enhanced robustness against fabrication damage. Another important component that calls for more research efforts are modulators, which have hitherto not been reported in single crystal diamond photonics. Since thermal tuning is not compatible with low-temperature operation required by coherent SPS and SNSPD, electromechanical modulation seems the most viable option. Beside photonic engineering, fundamental research for better understanding of diamond defects and the hunt for the discovery of new color centers are indispensable of a mature diamond photonics platform.

In summary, single crystal diamond diamond is one of the most promising quantum PIC platforms, and is today at the dawn of scalable design and manufacturing. Current advancements have already permitted integration with fiber-optics and with telecommunication infrastructure, and further development towards fully monolithic integration requires improvements on each step from crystal growth to device fabrication, which are believed to be within reach within the near future.

Acknowledgments

The authors acknowledge funding by the Swiss National Science Foundation under grants 157566 and 183717.

ORCID iD

Niels Quack https://orcid.org/0000-0001-5189-0929

References

[1] Mildren R P and Rabeau J R 2013 *Optical Engineering of Diamond: Mildren: Diamond Optics* (New York: Wiley)
[2] Hoffmann M M, Addleman R S and Fulton J L 2000 *Rev. Sci. Instrum.* **71** 1552–6
[3] Hirsch K R and Holzapfel W B 1981 *Rev. Sci. Instrum.* **52** 52–5
[4] Granados E, Spence D J and Mildren R P 2011 *Opt. Express* **19** 10857
[5] Latawiec P, Venkataraman V, Shams-Ansari A, Markham M and Lončar M 2018 *Opt. Lett.* **43** 318
[6] Reilly S, Savitski V G, Liu H, Gu E, Dawson M D and Kemp A J 2015 *Opt. Lett.* **40** 930
[7] Sabella A, Piper J A and Mildren R P 2014 *Opt. Lett.* **39** 4037

[8] Williams R J *et al* 2018 *IEEE J. Sel. Top. Quantum Electron.* **24** 1–14
[9] Kurtsiefer C, Mayer S, Zarda P and Weinfurter H 2000 *Phys. Rev. Lett.* **85** 290–3
[10] Aharonovich I and Neu E 2014 *Adv. Opt. Mater.* **2** 911–28
[11] Zaitsev A M 2001 *Optical Properties of Diamond: A Data Handbook* (Berlin: Springer)
[12] Hong S, Grinolds M S, Pham L M, Le Sage D, Luan L, Walsworth R L and Yacoby A 2013 *MRS Bull.* **38** 155–61
[13] Chang K, Eichler A, Rhensius J, Lorenzelli L and Degen C L 2017 *Nano Lett.* **17** 2367–73
[14] Maurer P C *et al* 2012 *Science* **336** 1283–6
[15] Bernien H *et al* 2013 *Nature* **497** 86–90
[16] Hess P 2012 *J. Appl. Phys.* **111** 051101
[17] Butler J E and Sumant A V 2008 *Chem. Vapor Depos.* **14** 145–60
[18] Hopcroft M A, Nix W D and Kenny T W 2010 *J. Microelectromech. Syst.* **19** 229–38
[19] Bhushan B and Li X 1997 *J. Mater. Res.* **12** 54–63
[20] Rath P, Ummethala S, Nebel C and Pernice W H P 2015 *Physica Status Solidi (a)* **212** 2385–99
[21] Okada Y and Tokumaru Y 1984 *J. Appl. Phys.* **56** 314–20
[22] Parker J H, Feldman D W and Ashkin M 1967 *Phys. Rev.* **155** 712–14
[23] Dréau A, Tcheborateva A, Mahdaoui A E, Bonato C and Hanson R 2018 *Phys. Rev. Appl.* **9** 064031
[24] Ikuta R *et al* 2014 *Opt. Express* **22** 11205
[25] Gould M, Schmidgall E R, Dadgostar S, Hatami F and Fu K M C 2016 *Phys. Rev. Appl.* **6** 011001
[26] Dolde F *et al* 2011 *Nat. Phys.* **7** 459–63
[27] Maletinsky P, Hong S, Grinolds M S, Hausmann B, Lukin M D, Walsworth R L, Loncar M and Yacoby A 2012 *Nat. Nanotechnol.* **7** 320–4
[28] Childress L and Hanson R 2013 *MRS Bull.* **38** 134–8
[29] Nguyen C T *et al* 2019 *Phys. Rev.* B **100** 165428
[30] Sumiya H and Tamasaku K 2012 *Japan. J. Appl. Phys.* **51** 090102
[31] Silva F, Achard J, Brinza O, Bonnin X, Hassouni K, Anthonis A, De Corte K and Barjon J 2009 *Diam. Relat. Mater.* **18** 683–97
[32] Polyakov S, Denisov V, Kuzmin N V, Kuznetsov M, Martyushov S, Nosukhin S, Terentiev S and Blank V 2011 *Diam. Relat. Mater.* **20** 726–8
[33] Palyanov Y N, Kupriyanov I N and Borzdov Y M 2019 *Carbon* **143** 769–75
[34] Balmer R S *et al* 2009 *J. Phys.: Condens. Matter.* **21** 364221
[35] Koizumi S, Umezawa H, Pernot J and Suzuki M 2018 Diamond wafer technologies for semiconductor device applications *Power Electronics Device Applications of Diamond Semiconductors* (Amsterdam: Elsevier) pp 1–97
[36] Schreck M, Asmussen J, Shikata S, Arnault J C and Fujimori N 2014 *MRS Bull.* **39** 504–10
[37] Yamada H, Chayahara A, Mokuno Y, Tsubouchi N and Shikata S i 2013 *Diam. Relat. Mater.* **33** 27–31
[38] Liang Q, Yan C s, Lai J, Meng Y f, Krasnicki S, Shu H, Mao H k and Hemley R J 2014 *Crystal Growth Design* **14** 3234–8
[39] Ichikawa K, Kurone K, Kodama H, Suzuki K and Sawabe A 2019 *Diam. Relat. Mater.* **94** 92–100
[40] Ichikawa K, Kodama H, Suzuki K and Sawabe A 2016 *Thin Solid Films* **600** 142–5
[41] Friel I, Clewes S, Dhillon H, Perkins N, Twitchen D and Scarsbrook G 2009 *Diam. Relat. Mater.* **18** 808–15
[42] Millar P, Birch R B, Kemp A J and Burns D 2008 *IEEE J. Quantum Electron.* **44** 709–17
[43] Takeuchi D, Makino T, Kato H, Ogura M, Tokuda N, Matsumoto T, Kuwabara D, Okushi H and Yamasaki S 2014 *Physica Status Solidi (a)* **211** 2251–6
[44] Nelz R *et al* 2019 *APL Mater.* **7** 011108
[45] Arend C *et al* 2016 *Appl. Phys. Lett.* **108** 063111
[46] Dai B *et al* 2017 *Diam. Relat. Mater.* **73** 204–9
[47] Aharonovich I, Lee J C, Magyar A P, Bracher D O and Hu E L 2013 *Laser Photon. Rev.* **7** L61–L65
[48] Schreck M, Gsell S, Brescia R and Fischer M 2017 *Sci. Rep.* **7** 44462
[49] Mi S, Toros A, Graziosi T and Quack N 2019 *Diam. Relat. Mater.* **92** 248–52
[50] Atikian H A, Eftekharian A, Jafari Salim A, Burek M J, Choy J T, Hamed Majedi A and Lončar M 2014 *Appl. Phys. Lett.* **104** 122602
[51] Ruf M, IJspeert M, van Dam S, de Jong N, van den Berg H, Evers G and Hanson R 2019 *Nano Lett.* **19** 3987–92
[52] Burek M J *et al* 2014 *Nat. Commun.* **5** 5718
[53] Sipahigil A *et al* 2016 *Science* **354** 847–50
[54] Tokuda N, Makino T, Inokuma T and Yamasaki S 2012 *Japan. J. Appl. Phys.* **51** 090107
[55] Okushi H, Watanabe H, Ri S, Yamanaka S and Takeuchi D 2002 *J. Cryst. Growth* **237-239** 1269–76
[56] Volpe P N, Muret P, Omnes F, Achard J, Silva F, Brinza O and Gicquel A 2009 *Diam. Relat. Mater.* **18** 1205–10
[57] Schuelke T and Grotjohn T A 2013 *Diam. Relat. Mater.* **32** 17–26
[58] Zheng Y *et al* 2020 *Diam. Relat. Mater.* **101** 107600
[59] Yamamura K, Emori K, Sun R, Ohkubo Y, Endo K, Yamada H, Chayahara A and Mokuno Y 2018 *CIRP Ann* **67** 353–6
[60] Hicks M L, Pakpour-Tabrizi A C and Jackman R B 2019 *Diam. Relat. Mater.* **97** 107424
[61] Rath P, Khasminskaya S, Nebel C, Wild C and Pernice W H 2013 *Beilstein J. Nanotechnol.* **4** 300–5
[62] Rath P, Khasminskaya S, Nebel C, Wild C and Pernice W H P 2013 *Nat. Commun.* **4** 1690
[63] Rath P, Gruhler N, Khasminskaya S, Nebel C, Wild C and Pernice W H P 2013 *Opt. Express* **21** 11031
[64] Faraon A, Barclay P E, Santori C, Fu K M C and Beausoleil R G 2011 *Nat. Photon.* **5** 301–5
[65] Burek M J *et al* 2012 *Nano Lett.* **12** 6084–9
[66] Khanaliloo B, Mitchell M, Hryciw A C and Barclay P E 2015 *Nano Lett.* **15** 5131–6
[67] Delaware Diamond Knives (www.ddk.com/index.php)
[68] Diamond Membranes & Foils | Applied Diamond, Inc
[69] Hausmann B J M, Bulu I B, Deotare P B, McCutcheon M, Venkataraman V, Markham M L, Twitchen D J and Lončar M 2013 *Nano Lett.* **13** 1898–902
[70] Hill P, Gu E, Dawson M D and Strain M J 2018 *Diam. Relat. Mater.* **88** 215–21
[71] Parikh N R *et al* 1992 *Appl. Phys. Lett.* **61** 3124
[72] Olivero P *et al* 2005 *Adv. Mater.* **17** 2427–30
[73] Marchywka M 1993 *J. Electrochem. Soc.* **140** L19
[74] Magyar A P, Lee J C, Limarga A M, Aharonovich I, Rol F, Clarke D R, Huang M and Hu E L 2011 *Appl. Phys. Lett.* **99** 081913
[75] Piracha A H, Ganesan K, Lau D W M, Stacey A, McGuinness L P, Tomljenovic-Hanic S and Prawer S 2016 *Nanoscale* **8** 6860–5

[76] Li L, Chen X, Zhang W and Peng K 2018 *Int. J. Refractory Metals Hard Mater.* **71** 129–34
[77] Sonin V M, Chepurov A I, Zhimulev E I, Chepurov A A and Sobolev N V 2013 *Doklady Earth Sciences* **451** 858–60
[78] Ralchenko V, Kononenko T, Pimenov S, Chernenko N, Loubnin E, Armeyev V and Zlobin A 1993 *Diam. Relat. Mater.* **2** 904–9
[79] Mehedi H A, Hebert C, Ruffinatto S, Eon D, Omnes F and Gheeraert E 2012 *Nanotechnology* **23** 455302
[80] Nagai M, Nakanishi K, Takahashi H, Kato H, Makino T, Yamasaki S, Matsumoto T, Inokuma T and Tokuda N 2018 *Sci. Rep.* **8** 6687
[81] Joshi A and Nimmagadda R 1991 *J. Mater. Res.* **6** 1484–90
[82] Appel P, Neu E, Ganzhorn M, Barfuss A, Batzer M, Gratz M, Tschöpe A and Maletinsky P 2016 *Rev. Sci. Instrum.* **87** 063703
[83] Izak T, Kromka A, Babchenko O, Ledinsky M, Hruska K and Ververniotis E 2012 *Vacuum* **86** 799–802
[84] Yamada T, Yoshikawa H, Uetsuka H, Kumaragurubaran S, Tokuda N and Shikata S i 2007 *Diam. Relat. Mater.* **16** 996–9
[85] Ando Y, Nishibayashi Y, Kobashi K, Hirao T and Oura K 2002 *Diam. Relat. Mater.* **11** 824–7
[86] Forsberg P and Karlsson M 2013 *Opt. Express* **21** 2693
[87] Challier M *et al* 2018 *Micromachines* **9** 148
[88] Lee C, Gu E, Dawson M, Friel I and Scarsbrook G 2008 *Diam. Relat. Mater.* **17** 1292–6
[89] Leech P W, Reeves G K, Holland A S and Shanks F 2002 *Diam. Relat. Mater.* **11** 833–6
[90] Atikian H A, Latawiec P, Burek M J, Sohn Y I, Meesala S, Gravel N, Kouki A B and Lončar M 2017 *APL Photonics* **2** 051301
[91] Pal P and Sato K 2017 *Silicon Wet Bulk Micromachining for MEMS* (Boca Raton, FL: CRC Press)
[92] Naamoun M, Tallaire A, Silva F, Achard J, Doppelt P and Gicquel A 2012 *Physica Status Solidi (a)* **209** 1715–20
[93] Tallaire A *et al* 2016 *Crystal Growth & Design* **16** 2741–6
[94] Mouradian S, Wan N H, Schröder T and Englund D 2017 *Appl. Phys. Lett.* **111** 021103
[95] Xie L, Zhou T X, Stöhr R J and Yacoby A 2018 *Adv. Mater.* **30** 1705501
[96] Rajput N S and Luo X 2015 Chapter 3 - FIB Micro-/Nano-fabrication *Micromanufacturing Engineering and Technology* Micro and Nano Technologies ed Qin Y (Boston, MA: William Andrew Publishing) 61–80
[97] Graziosi T, Mi S, Kiss M and Quack N 2018 *APL Photonics* **3** 126101
[98] Bharadwaj V *et al* 2019 *J. Phys. Photon.* **1** 022001
[99] Jin H, Turaga S P, Vanga S K and Bettiol A A 2018 *Opt. Lett.* **43** 2648–51
[100] Radtke M, Bernardi E, Slablab A, Nelz R and Neu E 2019 arXiv:1909.03719
[101] Doherty M W, Manson N B, Delaney P, Jelezko F, Wrachtrup J and Hollenberg L C 2013 *Phys. Rep.* **528** 1–45
[102] Bradac C, Gao W, Forneris J, Trusheim M and Aharonovich I 2019 arXiv:1906.10992
[103] Dresselhaus M S and Kalish R 1992 *Ion Implantation in Diamond, Graphite and Related Materials* Springer Series in Materials Science (Berlin: Springer) vol 22
[104] Ziegler J F, Ziegler M and Biersack J 2010 *Nucl. Instrum. Methods Phys. Res.* B vol 268 pp 1818–23
[105] Naydenov B, Reinhard F, Lämmle A, Richter V, Kalish R, D'Haenens-Johansson U F S, Newton M, Jelezko F and Wrachtrup J 2010 *Appl. Phys. Lett.* **97** 242511
[106] van Dam S B *et al* 2019 *Phys. Rev.* B **99** 161203(R)
[107] Orwa J O *et al* 2011 *J. Appl. Phys.* **109** 083530
[108] Lekavicius I and Wang H 2019 *Opt. Express* **27** 31299
[109] Evans R E, Sipahigil A, Sukachev D D, Zibrov A S and Lukin M D 2016 *Phys. Rev. Appl.* **5** 044010
[110] Schwartz J, Aloni S, Ogletree D F, Tomut M, Bender M, Severin D, Trautmann C, Rangelow I W and Schenkel T 2014 *J. Appl. Phys.* **116** 214107
[111] Schröder T *et al* 2017 *Nat. Commun.* **8** 15376
[112] Schukraft M, Zheng J, Schröder T, Mouradian S L, Walsh M, Trusheim M E, Bakhru H and Englund D R 2016 *APL Photonics* **1** 020801
[113] Pezzagna S *et al* 2010 *Small* **6** 2117–21
[114] Staudacher T, Ziem F, Häussler L, Stöhr R, Steinert S, Reinhard F, Scharpf J, Denisenko A and Wrachtrup J 2012 *Appl. Phys. Lett.* **101** 212401
[115] Lesik M *et al* 2016 *Physica Status Solidi (a)* **213** 2594–600
[116] Rugar A E, Lu H, Dory C, Sun S, McQuade P J, Shen Z X, Melosh N A and Vučković J 2019 arXiv:1910.14165
[117] Lehtinen O *et al* 2016 *Physical Review B* **93** 035202
[118] Fávaro de Oliveira F, Antonov D, Wang Y, Neumann P, Momenzadeh S A, Häuß ermann T, Pasquarelli A, Denisenko A and Wrachtrup J 2017 *Nat. Commun.* **8** 15409
[119] Farfurnik D, Alfasi N, Masis S, Kauffmann Y, Farchi E, Romach Y, Hovav Y, Buks E and Bar-Gill N 2017 *Appl. Phys. Lett.* **111** 123101
[120] Schwartz J, Aloni S, Ogletree D F and Schenkel T 2012 *New J. Phys.* **14** 043024
[121] McLellan C A, Myers B A, Kraemer S, Ohno K, Awschalom D D and Bleszynski Jayich A C 2016 *Nano Lett.* **16** 2450–4
[122] Rong Y *et al* 2019 *Opt. Lett.* **44** 3793
[123] Liu Y, Chen G, Song M, Ci X, Wu B, Wu E and Zeng H 2013 *Opt. Express* **21** 12843
[124] Chen Y C *et al* 2017 *Nat. Photon.* **11** 77–80
[125] Chen Y C *et al* 2019 *Optica* **6** 662
[126] Stephen C J *et al* 2018 *Phys. Rev. Appl.* **12** 064005
[127] Castelletto S, Edmonds A, Gaebel T and Rabeau J 2012 *IEEE J. Sel. Top. Quantum Electron.* **18** 1792–8
[128] Rabeau J R, Chin Y L, Prawer S, Jelezko F, Gaebel T and Wrachtrup J 2005 *Appl. Phys. Lett.* **86** 131926
[129] Orwa J, Greentree A, Aharonovich I, Alves A, Van Donkelaar J, Stacey A and Prawer S 2010 *J. Lumin.* **130** 1646–54
[130] Orwa J O, Aharonovich I, Jelezko F, Balasubramanian G, Balog P, Markham M, Twitchen D J, Greentree A D and Prawer S 2010 *J. Appl. Phys.* **107** 093512
[131] Ishiwata H, Nakajima M, Tahara K, Ozawa H, Iwasaki T and Hatano M 2017 *Appl. Phys. Lett.* **111** 043103
[132] Pham L M, Bar-Gill N, Le Sage D, Belthangady C, Stacey A, Markham M, Twitchen D J, Lukin M D and Walsworth R L 2012 *Phys. Rev.* B **86** 121202(R)
[133] Herbschleb E D *et al* 2019 *Nat. Commun.* **10** 3766
[134] Balasubramanian G *et al* 2009 *Nat. Mater.* **8** 383–7
[135] Lee J C *et al* 2014 *Appl. Phys. Lett.* **105** 261101
[136] Edmonds A M, D'Haenens-Johansson U F S, Cruddace R J, Newton M E, Fu K M C, Santori C, Beausoleil R G, Twitchen D J and Markham M L 2012 *Phys. Rev.* B **86** 035201

[137] Ohashi K *et al* 2013 *Nano Lett.* **13** 4733–8
[138] Rose B C *et al* 2018 *Science* **361** 60–3
[139] Jahnke K D, Sipahigil A, Binder J M, Doherty M W, Metsch M, Rogers L J, Manson N B, Lukin M D and Jelezko F 2015 *New J. Phys.* **17** 043011
[140] Doi Y *et al* 2016 *Phys. Rev.* B **93** 081203(R)
[141] Groot-Berning K *et al* 2014 *Physica Status Solidi (a)* **211** 2268–73
[142] D'Haenens-Johansson U F S, Edmonds A M, Green B L, Newton M E, Davies G, Martineau P M, Khan R U A and Twitchen D J 2011 *Phys. Rev.* B **84** 245208
[143] Hauf M V *et al* 2011 *Phys. Rev.* B **83** 081304(R)
[144] Shanley T W, Martin A A, Aharonovich I and Toth M 2014 *Appl. Phys. Lett.* **105** 063103
[145] Siyushev P, Pinto H, Vörös M, Gali A, Jelezko F and Wrachtrup J 2013 *Phys. Rev. Lett.* **110** 167402
[146] Doi Y *et al* 2014 *Phys. Rev.* **4** 011057
[147] McKnight L J, Dawson M D and Calvez S 2011 *IEEE J. Quantum Electron.* **47** 1069–77
[148] Grote R R and Bassett L C 2016 *APL Photon.* **1** 071302
[149] Courvoisier A, Booth M J and Salter P S 2016 *Appl. Phys. Lett.* **109** 031109
[150] Latawiec P, Shams-Ansari A, Okawachi Y, Venkataraman V, Yu M, Atikian H, Harris G L, Picqué N, Gaeta L and Loncar M 2018 Supercontinuum generation in angle-etched diamond waveguides *2018th Conf. on Lasers and Electro-Optics (CLEO)* 1–2
[151] Sotillo B *et al* 2016 *Sci. Rep.* **6** 35566
[152] Hadden J P *et al* 2018 *Opt. Lett.* **43** 3586–9
[153] Bharadwaj V, Wang Y, Fernandez T T, Ramponi R, Eaton S M and Galzerano G 2018 *Opt. Mater.* **85** 183–5
[154] Zhang Y, McKnight L, Tian Z, Calvez S, Gu E and Dawson M D 2011 *Diam. Relat. Mater.* **20** 564–7
[155] Hausmann B J M, Bulu I, Venkataraman V, Deotare P and Lončar M 2014 *Nat. Photon.* **8** 369–74
[156] Gao F, Van Erps J, Huang Z, Thienpont H, Beausoleil R G and Vermeulen N 2018 *IEEE J. Sel. Top. Quantum Electron.* **24** 1–9
[157] Gao F, Huang Z, Feigel B, Van Erps J, Thienpont H, Beausoleil R G and Vermeulen N 2016 *J. Lightwave Technol.* **34** 5576–82
[158] Hiscocks M P, Ganesan K, Gibson B C, Huntington S T, Ladouceur F and Prawer S 2008 *Opt. Express* **16** 19512–19
[159] Piracha A H, Rath P, Ganesan K, Kühn S, Pernice W H P and Prawer S 2016 *Nano Lett.* **16** 3341–7
[160] Latawiec P, Venkataraman V, Burek M J, Hausmann B J M, Bulu I and Lončar M 2015 *Optica* **2** 924
[161] Hausmann B J M *et al* 2012 *Nano Lett.* **12** 1578–82
[162] Gao F, Erps J V, Huang Z, Thienpont H, Beausoleil R G and Vermeulen N 2018 *J. Phys. Photon.* **1** 015003
[163] Gao F, Van Erps J, Huang Z, Thienpont H, Beausoleil R G and Vermeulen N 2018 *IEEE J. Sel. Top. Quantum Electron.* **24** 1–9
[164] Latawiec P, Venkataraman V, Burek M J, Hausmann B J M, Bulu I and Lončar M 2015 *Optica* **2** 924
[165] Burek M J *et al* 2017 *Phys. Rev. Appl.* **8** 024026
[166] Dory C *et al* 2019 *Nat. Commun.* **10** 1–7
[167] Shams-Ansari A *et al* 2019 arXiv:1906.08830
[168] Bayn I, Meyler B, Salzman J and Kalish R 2011 *New J. Phys.* **13** 025018
[169] Babinec T M, Choy J T, Smith K J M, Khan M and Lončar M 2011 *J. Vac. Sci. Technol.* B **29** 010601
[170] Schaffer M, Schaffer B and Ramasse Q 2012 *Ultramicroscopy* **114** 62–71
[171] Li L, Schröder T, Chen E H, Bakhru H and Englund D 2015 *Photon. Nanostruct. - Fundamentals Appl.* **15** 130–6
[172] Mitchell M, Lake D P and Barclay P E 2019 *APL Photonics* **4** 016101
[173] Wan N H, Mouradian S and Englund D 2018 *Appl. Phys. Lett.* **112** 141102
[174] Riedrich-Möller J *et al* 2012 *Nat. Nanotechnol.* **7** 69–74
[175] Hausmann B J M *et al* 2013 *Nano Lett.* **13** 5791–6
[176] Jung T, Kreiner L, Pauly C, Mücklich F, Edmonds A M, Markham M and Becher C 2016 *Physica Status Solidi (a)* **213** 3254–64
[177] Li L, Bayn I, Lu M, Nam C Y, Schröder T, Stein A, Harris N C and Englund D 2015 *Sci. Rep.* **5** 7802
[178] Burek M J *et al* 2016 *Optica* **3** 1404
[179] Mitchell M, Khanaliloo B, Lake D P, Masuda T, Hadden J P and Barclay P E 2016 *Optica* **3** 963
[180] Tao Y, Boss J M, Moores B A and Degen C L 2014 *Nat. Commun.* **5** 3638
[181] Chia C, Meesala S, El-Sawah N, Machielse B, Burek M J and Lončar M 2018 Diamond Optomechanical Crystals at Cryogenic Temperatures *Conf. on Lasers and Electro-Optics* (San Jose, CA: OSA) p SF2J.2
[182] Lake D P, Mitchell M, Kamaliddin Y and Barclay P E 2018 *ACS Photon.* **5** 782–7
[183] Lake D P, Mitchell M and Barclay P E 2018 *Front. Opt.* **2** FW7B.2
[184] Mitchell M, Lake D P and Barclay P E 2019 All optical control of pulse storage time and retrieval phase using a diamond microdisk *Conf. on Lasers and Electro-Optics* (San Jose, CA: OSA) p STh1H.4
[185] Mitchell M, Lake D P and Barclay P E 2018 Optomechanically mediated wavelength conversion in diamond microdisks *Conf. on Lasers and Electro-Optics* (San Jose, CA: OSA) p SF2J.1
[186] Mitchell M, Lake D P and Barclay P E 2019 arXiv:1902.07763
[187] Makino T *et al* 2011 *Appl. Phys. Lett.* **99** 061110
[188] Soltani M, Soref R, Palacios T and Englund D 2016 *Opt. Express* **24** 25415
[189] Maity S, Shao L, Sohn Y I, Meesala S, Machielse B, Bielejec E, Markham M and Lončar M 2018 *Phys. Rev. Appl.* **10** 024050
[190] Kato H, Wolfer M, Schreyvogel C, Kunzer M, Müller-Sebert W, Obloh H, Yamasaki S and Nebel C 2013 *Appl. Phys. Lett.* **102** 151101
[191] Aharonovich I, Castelletto S, Simpson D A, Su C H, Greentree A D and Prawer S 2011 *Rep. Prog. Phys.* **74** 076501
[192] Bernien H, Childress L, Robledo L, Markham M, Twitchen D and Hanson R 2012 *Phys. Rev. Lett.* **108** 043604
[193] Acosta V M *et al* 2012 *Phys. Rev. Lett.* **108** 206401
[194] Meesala S *et al* 2018 *Phys. Rev.* B **97** 205444
[195] Machielse B *et al* 2019 *Phys. Rev.* **9** 031022
[196] Sohn Y I *et al* 2018 *Nat. Commun.* **9** 2012
[197] Gould M, Chakravarthi S, Christen I R, Thomas N, Dadgostar S, Song Y, Lee M L, Hatami F and Fu K M C 2016 *J. Opt. Soc. Am.* B **33** B35
[198] Zhang J L *et al* 2018 *Nano Lett.* **18** 1360–5
[199] Riedrich-Möller J, Arend C, Pauly C, Mücklich F, Fischer M, Gsell S, Schreck M and Becher C 2014 *Nano Lett.* **14** 5281–7
[200] Faraon A, Santori C, Huang Z, Fu K M C, Acosta V M, Fattal D and Beausoleil R G 2013 *New J. Phys.* **15** 025010
[201] Faraon A, Barclay P E, Santori C, Fu K M C and Beausoleil R G 2011 *Nat. Photon.* **5** 301–5

[202] Mouradian S L 2018 A scalable quantum computation platform: solid state quantum memories coupled to photonic integrated circuits *PhD Thesis* Massachusetts Institute of Technology (http://hdl.handle.net/1721.1/118096)
[203] Wan N H, Shields B J, Kim D, Mouradian S, Lienhard B, Walsh M, Bakhru H, Schröder T and Englund D 2018 *Nano Lett.* **18** 2787–93
[204] Li L *et al* 2015 *Nano Lett.* **15** 1493–7
[205] Babinec T M, Hausmann B J M, Khan M, Zhang Y, Maze J R, Hemmer P R and Lončar M 2010 *Nat. Nanotechnol.* **5** 195–9
[206] Riedel D, Söllner I, Shields B J, Starosielec S, Appel P, Neu E, Maletinsky P and Warburton R J 2017 *Phys. Rev.* **7** 031040
[207] Mizuochi N *et al* 2012 *Nat. Photon.* **6** 299–303
[208] Lohrmann A, Pezzagna S, Dobrinets I, Spinicelli P, Jacques V, Roch J F, Meijer J and Zaitsev A M 2011 *Appl. Phys. Lett.* **99** 251106
[209] Bray K *et al* 2018 *Nanoscale* **10** 4028–35
[210] Berhane A M, Choi S, Kato H, Makino T, Mizuochi N, Yamasaki S and Aharonovich I 2015 *Appl. Phys. Lett.* **106** 171102
[211] Melnikov A A, Denisenko A V, Zaitsev A M, Shulenkov A, Varichenko V S, Filipp A R, Dravin V A, Kanda H and Fahrner W R 1998 *J. Appl. Phys.* **84** 6127–34
[212] Takeuchi D, Watanabe H, Yamanaka S, Okushi H, Sawada H, Ichinose H, Sekiguchi T and Kajimura K 2001 *Phys. Rev.* B **63** 245328
[213] Zaitsev A M, Bergman A A, Gorokhovsky A A and Huang M 2006 *Physica Status Solidi (a)* **203** 638–42
[214] Rand S C and DeShazer L G 1985 *Opt. Lett.* **10** 481
[215] Hammerling P, Budgor A B, Pinto A and Schawlow A L 1985 *Tunable Solid State Lasers: Proc. of the First Int. Conf. La Jolla, Calif. June 13–15, 1984* vol 47 (Berlin: Springer)
[216] Nakashima T and Yazu S 1990 Optical properties and laser action of H3 center in synthetic diamond *SPIE Proc.* **1325** 10–16
[217] Lin L T S, Prelas M A and Popovici G 1995 Laser Modes in Diamond *Wide Band Gap Electronic Materials* (Dordrecht: Springer) pp 187–206
[218] Neves A, Nazaré M, service I I, Group I E and Electrical Engineers I 2001 *Properties, Growth and Applications of Diamond* EMIS (Institution of Electrical Engineers) (https://books.google.ch/books?id=jtC1mUFZfQcC)
[219] Subedi S D, Fedorov V V, Peppers J, Martyshkin D V, Mirov S B, Shao L and Loncar M 2019 *Opt. Mater. Express* **9** 2076
[220] Vins V and Pestryakov E 2006 *Diam. Relat. Mater.* **15** 569–71
[221] Lu Y J, Lin C N and Shan C X 2018 *Adv. Opt. Mater.* **6** 1800359
[222] Chen Y C, Lu Y J, Lin C N, Tian Y Z, Gao C J, Dong L and Shan C X 2018 *J. Mater. Chem.* C **6** 5727–32
[223] Lin C, Lu Y, Tian Y, Gao C, Fan M, Yang X, Dong L and Shan C 2019 *Opt. Express* **27** 29962–71
[224] Webster S, Chen Y, Turri G, Bennett A, Wickham B and Bass M 2015 *J. Opt. Soc. Am.* B **32** 479
[225] Rohrer E, Nebel C, Stutzmann M, Flöter A, Zachai R, Jiang X and Klages C P 1998 *Diam. Relat. Mater.* **7** 879–83
[226] Kukushkin V, Lobaev M, Bogdanov S, Stepanov A, Kraev S, Okhapkin A, Arkhipova E, Zdoroveyshchev A and Ved M 2019 *Diam. Relat. Mater.* **97** 107444
[227] Liao M, Sang L, Teraji T, Imura M, Alvarez J and Koide Y 2012 *Japan. J. Appl. Phys.* **51** 090115
[228] Bevilacqua M and Jackman R B 2009 *Appl. Phys. Lett.* **95** 243501
[229] Chang X *et al* 2018 *Appl. Phys. Lett.* **112** 032103
[230] Atikian H A *et al* 2017 *SPIE Newsroom* (https://spie.org/news/6765-novel-fabrication-of-diamond-nanophotonics-coupled-to-single-photon-detectors)
[231] Rath P *et al* 2015 *Sci. Appl.* **4** e338–e338 *Light:*
[232] Kahl O, Ferrari S, Rath P, Vetter A, Nebel C and Pernice W H P 2016 *J. Lightwave Technol.* **34** 249–55
[233] Rath P, Vetter A, Kovalyuk V, Ferrari S, Kahl O, Nebel C, Goltsman G N, Korneev A and Pernice W H P 2016 Travelling-wave single-photon detectors integrated with diamond photonic circuits: Operation at visible and telecom wavelengths with a timing jitter down to 23 ps *SPIE OPTO* (*San Francisco, California, United States*) p 97500T
[234] Rath P, Ummethala S, Diewald S, Lewes-Malandrakis G, Brink D, Heidrich N, Nebel C and Pernice W H P 2014 *Appl. Phys. Lett.* **105** 251102
[235] Murai T *et al* 2018 *Appl. Phys. Lett.* **112** 111903
[236] Forneris J *et al* 2017 *Carbon* **113** 76–86
[237] Siyushev P *et al* 2019 *Science* **363** 728–31
[238] Bourgeois E, Jarmola A, Siyushev P, Gulka M, Hruby J, Jelezko F, Budker D and Nesladek M 2015 *Nat. Commun.* **6** 8577
[239] Bourgeois E *et al* 2017 *Physical Review B* **95** 041402(R)
[240] Ovartchaiyapong P, Lee K W, Myers B A and Jayich A C B 2014 *Nat. Commun.* **5** 4429
[241] Maity S *et al* 2019 arXiv:1910.09710
[242] Golter D A, Oo T, Amezcua M, Stewart K A and Wang H 2016 *Phys. Rev. Lett.* **116** 143602
[243] Meesala S, Sohn Y I, Atikian H A, Kim S, Burek M J, Choy J T and Lončar M 2016 *Phys. Rev. Appl.* **5** 034010
[244] Wang Y, Kong M, Xu Y and Zhou Z 2018 *J. Opt.* **20** 025801
[245] Wolf R, Breunig I, Zappe H and Buse K 2018 *Opt. Express* **26** 19815
[246] Bogaerts W and Selvaraja S K 2011 *IEEE Photonics J.* **3** 422–32
[247] Bray K *et al* 2018 *Nanoscale* **10** 4028–35
[248] Khanaliloo B, Jayakumar H, Hryciw A C, Lake D P, Kaviani H and Barclay P E 2015 *Phys. Rev.* **5** 041051
[249] Wu H *et al* 2018 *Phys. Rev. Mater.* **2** 090601
[250] Barson M S J *et al* 2017 *Nano Lett.* **17** 1496–503
[251] Kepesidis K V, Bennett S D, Portolan S, Lukin M D and Rabl P 2013 *Phys. Rev.* B **88** 064105
[252] Barfuss A, Teissier J, Neu E, Nunnenkamp A and Maletinsky P 2015 *Nat. Phys.* **11** 820–4
[253] Lemonde M A, Meesala S, Sipahigil A, Schuetz M J A, Lukin M D, Loncar M and Rabl P 2018 *Phys. Rev. Lett.* **120** 213603
[254] Ummethala S, Rath P, Lewes-Malandrakis G, Brink D, Nebel C and Pernice W 2014 *Diam. Relat. Mater.* **44** 49–53
[255] Bassett L C, Heremans F J, Yale C G, Buckley B B and Awschalom D D 2011 *Phys. Rev. Lett.* **107** 266403
[256] Sipahigil A, Goldman M L, Togan E, Chu Y, Markham M, Twitchen D J, Zibrov A S, Kubanek A and Lukin M D 2012 *Phys. Rev. Lett.* **108** 143601
[257] Lozovik A, Tordjman M, Meyler B, Bayn I, Salzman J and Kalish R 2016 *J. Appl. Phys.* **120** 163107
[258] Jeske J *et al* 2017 *Nat. Commun.* **8** 14000
[259] Fraczek E *et al* 2017 *Opt. Mater. Express* **7** 2571
[260] Jeske J, Cole J H and Greentree A D 2016 *New J. Phys.* **18** 013015
[261] Kerman A J, Dauler E A, Yang J K W, Rosfjord K M, Anant V, Berggren K K, Gol'tsman G N and Voronov B M 2007 *Appl. Phys. Lett.* **90** 101110

[262] Akhlaghi M K, Atikian H, Eftekharian A, Loncar M and Majedi A H 2012 *Opt. Express* **20** 23610
[263] Ilin K, Henrich D, Luck Y, Liang Y, Siegel M and Vodolazov D Y 2014 *Phys. Rev.* B **89** 184511
[264] Charaev I, Semenov A, Ilin K and Siegel M 2019 *IEEE Trans. Appl. Supercond.* **29** 1–5
[265] Tillmann M, Dakić B, Heilmann R, Nolte S, Szameit A and Walther P 2013 *Nat. Photon.* **7** 540–4
[266] Spring J B *et al* 2013 *Science* **339** 798–801
[267] Knill E, Laflamme R and Milburn G J 2001 *Nature* **409** 46–52
[268] Okamoto R, O'Brien J L, Hofmann H F and Takeuchi S 2011 *Proc. Natl Acad. Sci.* **108** 10067–71